UNIVERSIDADE FEDERAL DE MINAS GERAIS
Escola de Engenharia
Programa de Pós-Graduação em Engenharia Metalúrgica, Materiais e de Minas

Tese de Doutorado

O Processo de Redução Direta no Contexto da Descarbonização da Siderurgia e a Busca por Soluções Tecnológicas de Agentes de Recobrimento para Pelotas de Minério de Ferro

Autor: Jean Philippe Santos Gherardi de Alencar
Orientador: Wander Luiz Vasconcelos
Co-orientadora: Valdirene Gonzaga de Resende

Belo Horizonte
2021

Jean Philippe Santos Gherardi de Alencar

O Processo de Redução Direta no Contexto da Descarbonização da Siderurgia e a Busca por Soluções Tecnológicas de Agentes de Recobrimento para Pelotas de Minério de Ferro

Tese apresentada ao Programa de Pós-Graduação em Engenharia Metalúrgica, Materiais e de Minas da Escola de Engenharia da Universidade Federal de Minas Gerais, como requisito parcial para obtenção do Grau de Doutor em Engenharia Metalúrgica, Materiais e de Minas

Área de Concentração: Ciência e Engenharia de Materiais
Orientador: Wander Luiz Vasconcelos
Coorientadora: Valdirene Gonzaga de Resende

Belo Horizonte
Universidade Federal de Minas Gerais
Escola de Engenharia
2021

Alencar, Jean Philippe Santos Gherardi de.
A368p O processo de redução direta no contexto da descarbonização da siderurgia e a busca por soluções tecnológicas de agentes de recobrimento para pelotas de minério de ferro [recurso eletrônico] / Jean Philippe Santos Gherardi de Alencar. – 2021.
1 recurso online (x, 68 f. : il., color.) : pdf.

Orientador: Wander Luiz Vasconcelos.
Coorientadora: Valdirene Gonzaga Resende.

Tese (doutorado) - Universidade Federal de Minas Gerais, Escola de Engenharia.

Inclui bibliografia.
Exigências do sistema: Adobe Acrobat Reader.

1. Engenharia Metalúrgica - Teses. 2. Pelotização (Beneficiamento de minério) – Teses. 3. Redução de minérios - Teses. 4. Siderurgia – Teses. I. Vasconcelos, Wander Luiz. II. Resende, Valdirene Gonzaga. III. Universidade Federal de Minas Gerais. Escola de Engenharia. IV. Título.

CDU: 669(043)

Ficha catalográfica elaborada pela Bibliotecária Letícia Alves Vieira - CRB-6/2337
Biblioteca Prof. Mário Werneck - Escola de Engenharia da UFMG

UNIVERSIDADE FEDERAL DE MINAS GERAIS
ESCOLA DE ENGENHARIA
Programa de Pós-Graduação em Engenharia Metalúrgica, Materiais e de Minas

Tese intitulada **"O Processo de Redução Direta no Contexto da Descarbonização da Siderurgia e a Busca por Soluções Tecnológicas de Agentes de Recobrimento para Pelotas de Minério de Ferro"**, área de concentração: Ciência e Engenharia de Materiais, apresentada pelo candidato **Jean Philippe Santos Gherardi de Alencar**, para obtenção do grau de Doutor em Engenharia Metalúrgica, Materiais e de Minas, aprovada pela comissão examinadora constituída pelos seguintes membros:

Prof. Wander Luiz Vasconcelos
Orientador - PhD (UFMG)

Valdirene Gonzaga de Resende
Coorientador - Drª (VALE S.A.)

Prof. Maurício Covcevich Bagatini
Dr. (UFMG)

Bruno Amaral Pereira
Dr. (VALE)

Profª Jéssica de Oliveira Notório Ribeiro
Drª (UFLA)

Fabrício Parreira
Dr. (VALE S.A.)

Rodrigo Lambert Oréfice
Coordenador do Programa de Pós-Graduação em Engenharia Metalúrgica, Materiais e de Minas/UFMG

Belo Horizonte, 17 de dezembro de 2021

Dedico este trabalho à toda minha família e em especial aos meus pais, à minha esposa e ao meu filho Vitor.

AGRADECIMENTOS

Primeiramente a DEUS.

A minha esposa Marcela e ao meu filho Vitor pelo carinho, companheirismo, e compreensão quanto a necessidade de momentos de isolamento e foco no trabalho.

A minha Mãe e a meu Pai (*in memoriam*) pela educação, valores, incentivo e amor. Ao meu irmão Rodrigo pela força e tranquilidade.

A Universidade Federal de Minas Gerais pela oportunidade de aperfeiçoamento profissional.

A CAPES/PROEX, FAPEMIG e CNPq pelo apoio ao programa de pós-graduação PPGEM/UFMG.

Ao professor Wander Vasconcelos pelo acolhimento, apoio e orientação.

A Valdirene Resende pela mentoria, disponibilidade e comprometimento com o trabalho.

Aos colegas da Vale que trabalharam direta ou indiretamente nessa jornada de incremento de conhecimento técnico como Rogério Carneiro, Paulo Bandeira, Alei Domingues, Delciane Porfiro, Fabrício Parreira, Flávio Dutra, Pedro Rosa, Vinícius Morais, Washington Mafra, Emile Scheepers, Claudionor Antônio, Arlindo Maciel, Etevani Gomes, Ana Paula e Márcio Ricardo.

Aos parceiros e colaboradores dos trabalhos técnicos de simulação, professor José Adilson e Dr. Bruno Amaral.

Aos colegas orientandos do Laboratório de Materiais Cerâmicos da UFMG, em especial a Priscila Alves pela troca técnica e companheirismo.

RESUMO

A siderurgia mundial está diante de um desafio de descarbonização jamais visto antes, que implica em necessidades de desenvolvimento técnico e vultuosos dispêndios financeiros. Uma pesquisa de dados feita na primeira etapa deste trabalho mostrou que, algumas das principais usinas siderúrgicas da Europa, já sofrem com um déficit significativo entre as permissões e emissões verificadas de CO_2. Dentre as iniciativas que visam evitar tais emissões, foi notório o destaque para o maior uso da rota de Redução Direta como por exemplo nos projetos HYBRIT e SALCOS. Contudo, um aspecto importante para uso dessa rota é a susceptibilidade ao fenômeno da colagem que pelotas de minério de ferro apresentam, sendo que as pelotas são a principal carga metálica usada nos reatores. Com isso, na segunda e terceira etapa do estudo o foco foi discorrer sobre esse fenômeno que é crítico para a operacionalização técnica do processo de Redução Direta: o controle da colagem de pelotas. A fim de quantificar os impactos que a colagem causa a operação do reator, a segunda parte do trabalho foi dedicada à adaptação de um modelo numérico que representasse um forno do tipo cuba e todas as equações de conservação de massa, energia e momentum pertinentes ao processo. O diferencial desse estudo foi que ele levou em consideração outros estudos de simulação física a fim de promover equações e parametrizações que tornassem o modelo apto a simular essa queda de pressão em função da formação dos cachos. A seleção da melhor equação e parametrização foi tomada com base numa referência de impacto industrial cuja carga e Índice de Colagem eram conhecidos. Por sua vez, a terceira etapa do estudo contemplou um plano de trabalho laboratorial que visou identificar quais materiais e processos de aplicação de recobrimento para pelotas seriam mais efetivos no combate à colagem. Foi possível perceber que o uso da Bentonita combinado com materiais refratários propiciou melhor dispersão nas polpas e menor Índice de Colagem. Adicionalmente, constatou-se que o método de aplicação a seco na pelota crua foi pouco eficaz e isso pode ser explicado pela baixa quantidade de material na superfície da pelota após a queima. Dentre todos os parâmetros e testes realizados, obteve-se que o Índice de Adesão e a soma dos teores de SiO_2, Al_2O_3, CaO e MgO foram os mais influentes na variável resposta de Índice de Colagem. O Índice de Adesão foi também avaliado como variável dependente e observou-se que há uma relação forte entre os seus resultados e o da área superficial específica medida por adsorção de N_2 (método BET). A Bauxita foi o material que teve melhor desempenho nesse estudo e suas vantagens foram o alto teor de Al_2O_3 que lhe conferiu ótimas propriedades refratárias, confirmadas pelo teste de fusibilidade e a elevada superfície

específica. Por fim, uma etapa complementar de testes foi realizada a fim de otimizar os resultados da terceira etapa e conectá-los com a aplicação do modelo da segunda etapa. Percebeu-se que a aplicação de duas camadas de recobrimento, uma na pelota crua e outra na pelota queimada, seguida de tratamento térmico à 400 °C, propiciou um melhor resultado de Índice de Colagem. Contudo, os valores obtidos nessas otimizações não foram tão melhores que o valor de referência de uma aplicação simples de Bauxita numa pelota queimada. Ao se comparar o impacto dessas duas situações no modelo, uma com aplicação de Bauxita simples e a outra com aplicação dupla e tratamento térmico, o ganho de produção seria de apenas 0,3 t/h.

Palavras-chave: pelotas de minério de ferro; siderurgia; redução direta; recobrimento; colagem.

ABSTRACT

The world steel industry is facing a decarbonization challenge never seen before, which requires technical development and substantial financial expenses. A data survey carried out in the first stage of this work showed that some of the main steel mills in Europe already suffer from a significant deficit between the allowances and verified CO_2 emissions. The greater use of the Direct Reduction route like in the HYBRIT and SALCOS projects are some of the highlighted initiatives aiming to avoid such emissions. However, an important aspect for the use of this route is the susceptibility to the clustering that iron ore pellets, which are the main metallic charge used in the reactors, can present. Thus, in the second and third stages of the study, the focus was to discuss this phenomenon that is critical for the Direct Reduction technical operationalization process: the control of pellet clustering. In order to quantify the impacts caused by sticking on the reactor operation, the second part of the work was dedicated to the adaptation of a numerical model that represented a shaft furnace and all the equations of mass, energy and momentum conservation relevant to the process. The peculiarity of this study was that it took into account other physical simulation studies in order to promote equations and parameterizations that would make the model able to simulate this pressure drop due to the cluster's formation. The selection of the best equation and parameterization was based on an industrial reference value whose burden and Clustering Index were known. Then, the third stage of the study included a large laboratory work plan that aimed to identify which materials and application processes for coating pellets would be more effective in preventing the sticking phenomenon. It was possible to see that the use of Bentonite combined with other refractory materials provided a better Dispersion Degree in the pulps and a lower Clustering Index. Additionally, it was found that the dry application method on the green pellet was ineffective, and this can be explained by the low amount of material on the pellet surface after firing. Among all parameters and tests performed, it was found that the Adhesion Index and the sum of the SiO_2, Al_2O_3, CaO and MgO contents were the most influential in the Clustering Index response variable. The Adhesion Index was also evaluated as a dependent variable, and it was observed that there is a strong relationship between its results and the superficial area measured by N_2 adsorption (BET method). Bauxite was the material that performed best in this study, and it can be said that its advantages were the high content of Al_2O_3 that gave it excellent refractory properties, confirmed by the fusibility test and the high superficial area. Finally, a complementary test step was carried out in order to seek an optimization of the results of the

third step and connect these results with the application of the second step model. It was noticed that the application of two coating layers, one in the green pellet and the other in the fired pellet, provided a better Clustering Index results in the two cases evaluated. Furthermore, the use of a thermal treatment technique at 400 °C after the second layer was also beneficial to reduce the Clustering Index. However, the values obtained in these optimizations, although better, were not significantly lower than the reference value of a simple application of Bauxite in a fired pellet. When comparing the impact of these two situations on the numerical model, one with simple Bauxite application and the other with double application and heat treatment, the production gain would be only 0.3 t/h.

Keywords: iron ore pellets; ironmaking; direct reduction; coating; clustering.

SUMÁRIO

LISTA DE FIGURAS

LISTA DE TABELAS

LISTA DE SÍMBOLOS E ABREVIATURAS

DRI – *Direct Reduced Iron*

WSA - *World Steel Association*

DR – *Direct Reduction*

EAF – *Electric Arc Furnace*

BF – *Blast Furnace*

BOF – *Basic Oxygen Furnace*

CDA – *Carbon Direct Avoidance*

CCU – *Carbon Capture and Usage*

CCS – *Carbon Capture and Storage*

LOI - *Loss On Ignition*

PPC – Perda por Calcinação

PF – *Pellet Feed*

CMC – Carboxi-Metil-Celulose

IEA - *International Energy Agency*

RC – Resistência à Compressão

Met – Grau de Metalização

IC – Índice de Colagem

IA – Índice de Adesão

ISO – *International Standard Organization*

PRD – Pelota para o processo de Redução Direta

RD – Redução Direta

TG – Termogravimetria

DTA – Análise Térmica Diferencial

GD – Grau de Dispersão

GLP – Gás Liquefeito de Petróleo

CTF – Centro de Tecnologia de Ferrosos

MEV – Microcopio Eletrônico de Varredura

EDS – *Energy Dispersive Spectroscopy*

DRX – Difração de Raios-X

Capítulo 1. Considerações iniciais

1.1. Introdução

Vários países e regiões signatárias do Acordo de Paris têm estabelecido metas de redução de CO_2 que trazem consequências muito relevantes para suas respectivas produções de aço. Na Europa e alguns países da Ásia, é esperado que até 2050 as economias, incluindo a siderurgia, sejam carbono neutras. Nesse cenário, vários projetos novos de Redução Direta como o HYBRIT e o SALCOS vêm sendo lançados ao redor do mundo, devido a sua menor pegada de carbono em relação a rota Alto-Forno.

Dados de 2020 da MIDREX apontam que a produção de DRI (*Direct Reduced Iron*) no mundo já ultrapassou a incrível marca de 100 milhões de toneladas por ano, o que comprova o momento de expansão do segmento. Nesse contexto, pode-se destacar o acréscimo de produção em alguns países como EUA, Rússia, Egito, Irã e Índia. Na grande maioria dos países há a predominância de produção de DRI através de reatores de cuba com carga granular como as tecnologias desenvolvidas e conhecidas como Midrex e HyL. Aproximadamente, 76% da produção mundial é oriunda desses tipos de reatores.

Nessa conjectura, o papel das pelotas de minério de ferro é assaz importante, pois elas se apresentam como o tipo de carga mais indicado para a alimentação dos reatores de cuba. Um aspecto demasiadamente importante para o processo RD é a susceptibilidade ao fenômeno da colagem. Vários trabalhos já reportaram sobre esse assunto, retratando não apenas a ocorrência do mesmo em pelotas, mas também em finos utilizados em leitos fluidizados, onde o problema é ainda maior devido à elevada superfície específica.

A colagem se resume ao fenômeno de sinterização do ferro metálico, que se forma na superfície das partículas reduzidas e pode assumir diferentes morfologias, sendo essas as responsáveis pelas interações e ancoragens dessas partículas de maneira a formar aglomerados maiores e, por fim, causando os problemas conhecidos da colagem. As morfologias de ferro metálico mais comumente encontradas e, em ordem crescente de resistência mecânica, são: (i) erodido e poroso, (ii) ferro fibroso e alongado e (iii) ferro recém precipitado de alta energia com formato arredondado e liso. A temperatura e atmosfera gasosa são os parâmetros que mais influenciam para a determinação da morfologia. Em reatores RD de cuba, os cachos se formam na zona de redução, próxima às paredes e à medida que eles se desenvolvem começam a aparecer problemas como perda de permeabilidade, instabilidade operacional devido aos

distúrbios do fluxo gasoso, menor produtividade/metalização e em casos extremos leva a parada do reator para a remoção mecânica dos cachos e manutenção corretiva da estrutura interna.

Dentre as contramedidas existentes para minimizar a colagem de pelotas no interior dos reatores tem-se duas opções práticas: uma é a diminuição da temperatura dos gases redutores e a outra é o artifício do uso de agentes de recobrimento. A primeira citada é usada em momentos críticos, principalmente quando já se detecta a presença de cachos, porém não é aconselhada, pois, ao se trabalhar com temperaturas menores reduz-se a favorabilidade cinética de redução e, consequentemente, gera-se um produto (DRI) de menor qualidade. Logo, o uso de recobrimento com materiais refratários, usualmente dito como *coating* se transforma no principal subterfúgio para mitigar os problemas operacionais sem comprometer a qualidade final do ferro reduzido. Normalmente, a aplicação desse material se dá na forma de aspersão após preparação de uma polpa no momento intermediário onde a pelota se encontra na transição do forno para o pátio de empilhamento. Os materiais mais utilizados como *coating* são minerais óxidos ricos em elementos como SiO_2, Al_2O_3 e MgO. No entanto, apesar dos desenvolvimentos e esforços já feitos, o conhecimento acerca das possíveis interações entre materiais refratários simultaneamente aplicados com outros aditivos, bem como outras formas alternativas de aplicação do *coating* ainda não foram suficientemente explorados, o que impacta consideravelmente na busca por soluções mais efetivas. Além disso, a tendência futura de reatores maiores, com temperatura e pressão mais elevados também são fatores que endossam a importância dessas investigações.

Assim sendo, este trabalho visou se aprofundar no entendimento dos mecanismos e fenômenos envolvidos quando da aplicação de agentes de recobrimento sobre pelotas de minério de ferro que são consumidas em reatores RD e seus respectivos impactos no processo.

1.2.Objetivos

O objetivo geral do presente trabalho foi de melhor compreender os fundamentos que impactam na eficiência dos agentes de coating e à luz disso buscar quantificar as consequências operacionais no processo de redução direta. Logo, uma série de diferentes agentes de recobrimento e métodos de aplicação foram explorados em diferentes testes de caracterização e performance.

Os objetivos específicos deste trabalho foram de avaliar:

- o balanço das emissões de CO_2 verificadas e licenças para emitir de algumas das principais usinas siderúrgicas da Europa;
- as principais alternativas de redução de emissões que estão sendo cogitadas pela indústria siderúrgica;
- o impacto da formação de cachos no desempenho de reator de redução direta através de modelagem fluido dinâmica;
- a susceptibilidade ao amolecimento e fluidez dos materiais de *coating* quando expostos a altas temperaturas;
- o nível de dispersão das misturas de recobrimento em polpa;
- o impacto do método de aplicação do *coating* (na pelota crua ou queimada) na eficiência de recobrimento e prevenção à formação de cachos;
- a relação entre as características do material de recobrimento, método de aplicação e índice de colagem laboratorial.
- O impacto do tratamento térmico pós-aplicação de recobrimento no índice de colagem.

1.3. Estrutura da Tese e Descrição dos Artigos

A redação da presente tese fundamentou-se em três artigos internacionais: Artigo A (Capítulo 2), Artigo B (Capítulo 3) e Artigo C (Capítulo 4). Além dessas seções, o trabalho ainda conta com o presente capítulo que introduz o leitor ao tema e aos objetivos do estudo, com o capítulo de estudo complementar (Capítulo 5) no qual se tem uma etapa adicional do trabalho que explorou uma nova forma de aplicação de recobrimento avaliando sua otimização não apenas pelo viés do ensaio laboratorial, mas também pelo impacto no processo através do modelo numérico descrito no Capítulo 3 e, por fim, encontram-se os Capítulos 6, 7 e 8 que, respectivamente, apresentam as considerações finais, as principais contribuições originais do trabalho e as possíveis investigações futuras envolvendo o tema.

A seguir são citados os artigos que são corpo principal do presente trabalho:

- Artigo A - **The impact of the emission trading scheme on the European steel industry and the future trends for technologies for obtaining primary iron**: Nessa primeira etapa do trabalho aprofundou-se no contexto da descarbonização global que têm pressionado a indústria siderúrgica a fazer movimentos significativos de readequação de rotas. Tal contexto, com exemplos de siderúrgicas europeias mostra de forma latente a dimensão do problema e coloca entre as mais promissoras alternativas o maior uso da rota de redução direta e forno elétrico, o que reforça a importância de se estudar esse processo;
- Artigo B - **Evaluation of the impact of cluster formation in a direct reduction shaft furnace through numerical simulation**: Nesse artigo o foco foi ajustar um modelo de simulação numérica para torná-lo apto a estimar o impacto da formação dos cachos de colagem nos parâmetros de operação do forno, em especial na produtividade. A partir da comparação dos resultados teóricos com uma referência industrial foi possível estabelecer esse refinamento do modelo e calibrá-lo para simulações de outras cargas e agentes de recobrimento.
- Artigo C - **Effect of Coatings and Coating Methods on Cluster Index in Iron Oxide Pellets for Direct Reduction Shaft Furnaces**: Neste trabalho, procurou-se entender quais variáveis (materiais de coating e método de aplicação) e quais fundamentos e características delas seriam mais influentes no índice de colagem laboratorial. A abordagem permitiu fazer várias análises e gerou um conhecimento relevante para a seleção de materiais e futuros desenvolvimentos.

Capítulo 2. Artigo A - The impact of the emission trading scheme on the European steel industry and the future trends for technologies for obtaining primary iron

Jean Philippe Santos Gherardi de Alencar [a,*], *Valdirene Gonzaga de Resende* [a] *and Wander Luiz Vasconcelos*[b]

[a] Ferrous Technology Center, Vale S.A., Nova Lima, MG, Brazil

[b] Metallurgical Department, Federal University of Minas Gerais (UFMG), Belo Horizonte, MG, Brazil

* Corresponding author

Email: jeanpga@gmail.com

Artigo publicado pela revista Tecnologia em Metalurgia, Materiais e Mineração (TMM)

Submetido em: 01/07/2020 - Aceito em: 16/03/2021.

Tecnologia em Metalurgia, Materiais e Mineração, v. 18, p. 1-9, 2021

https://doi.org/10.4322/2176-1523.20212409

ABSTRACT

Climate change is often subject of discussions around the world that implies in several initiatives that support the reduction of greenhouse gases (GHG). Currently, countries that signed the Paris Agreement in 2015 have plans to restrict GHG emissions based on the NDC (Nationally Determined Contributions) established. These reductions are expected to come also from industries, including the steel one. Some countries and regions are highlighted for having more developed policies than the rest of the world, such as Europe, which since 2005 has been implementing an Emission Trading Scheme (ETS). In this context, the European steel industry has been facing challenges which impose a need for disruptive technology innovation. This work presents four different European steel mills from different countries. A variety of finished products were analyzed, and it was found that in all four cases there is a deficit between the verified GHG emissions and the licenses granted for emission. The specific emissions per ton of steel and energy efficiency of each plant play an important role in justifying these differences

in CO_2 balance among the plants. Therefore, there are multiple initiatives in progress involving steel producers in Europe that encourage the use of new technologies and modified routes to reduce and mitigate the volume of emissions in the steel production chain. The success of these initiatives from a technical and an economic point of view is the path to sustainability, competitiveness and value generation for the future industry.

Keywords: greenhouse gases, emissions, ironmaking, steelmaking.

2.1. Introduction

Climate change has become one of the most important issues in global politics. The Kyoto protocol, introduced in 1997, was the first international agreement to reduce GHG (Greenhouse Gases)[1]. The Paris agreement, signed in 2015 and valid since November 2016, aimed to limit climate change in this century to below 2 °C above pre-industrial levels and to pursue efforts to limit the temperature increase even further to 1.5 °C[2]. This agreement was ratified by 179 countries, which are in different stages of implementing/developing their policies[3]. This global consensus on the need to take action against climate change implies on the acceleration of policies and regulations that inevitably bring impacts to the industrial competitiveness of all countries and their respective economies[4].

In this context, the European Union (28 countries), Norway, Iceland and Liechtenstein have been committed to a regulated carbon market, the ETS (Emissions Trading Scheme), which aims to promote the reduction of GHG by 95 % until 2050 (compared to 1990 emission levels)[5]. According to the World Steel Association (2018), the global steel production accounts for approximately 7 to 9 % of direct CO_2 emissions[6] and, as a result, it is irrefutable that discussions about GHG reduction policies have a direct and deep impact on the steelmaking chain.

Thus, this work shows an approach of how GHG reduction policies takes place and how they have impacted steel industry and its competitiveness.

2.1.1 GHG Reduction Policies Around the World

Each of the signatory countries to the Paris agreement is at a different level of policies implementation that aim to reduce the number of GHG emissions. There are cases ranging from prohibiting emissions from certain sources, imposing taxes or fines for emissions beyond what is desirable and what has been most widely accepted in capitalist economies is the creation of emissions trading schemes. In this context, it is relevant to highlight the role of the ICAP (International Carbon Action Partnership), which is an international forum for governments and public authorities to exchange best practices, data and information regarding their carbon regulation systems and promote the discussions about a global credit carbon market[7].

Nowadays, Asia-Pacific (APAC) is the region that has the largest share of total carbon emissions regulated by implemented ETS systems, closely followed by Europe and less by the American continent. ICAP monitors these ETS systems, indexes and consolidates them on its web page. Through the quotes from January 2020, it is noted that while in some places like

Korea and Europe each 1 ton of CO_2 is quoted close to 30 USD, in other places like pilots' markets in China the quotation is around to 5 USD per ton[7].

Regardless the approach that each country has been following, the Paris agreement through the NDC established long-term goals that each signatory should honor in order to contribute to mitigating the impacts of climate changes. It is observed that countries have stipulated levels of reduction that are quite different from each other. The reduction proposed by Europe is quite audacious while China's reduction may not be proportionately high, but it will have a significant impact on the absolute number of tons of CO_2. On the other side, Brazil has assumed a goal of reducing emissions by 37% by 2025, based on the 2005 figures[8].

2.1.2 Context and Current Stage of European ETS

The European ETS has been implemented by steps. In 2005, it was initially launched as a pilot plan and now is in its third stage. The fourth stage begins in 2021, with a period extending from 2021 to 2030. The total regulated volume covers approximately 45% of all emissions in Europe. Sectors such as steel, thermoelectric, refineries, cement, refractories, glass, bricks, ceramics, paper and cellulose, electricity generators, combustion plants and airlines are included, accounting for more than 11,000 industrial installations[9].

The EU ETS limits overall GHG emissions of all participants in the system, in any given year, to a specific amount in tons of CO_2 equivalent (t CO_2e). CO_2e is a metric measure used to put the emissions from various GHG on similar basis according to their global-warming potential (GWP). The free allocations are defined each year to the exact the same number as the total GHG limit set for the year and it is distributed through auctions to participants in the system, who can also freely trade them amongst themselves. By April 30th of each year, participants must provide regulators with one allowance to cover each single ton of CO_2e they emitted in the previous year. Non-compliance results in a heavy fine of EUR 100/tCO_2e for each ton of emissions without the corresponding allowance[5]. Since the third stage of ETS Europe, emission allowances were distributed to Member States using a benchmark formula applied at the installation level. This calculation considers five components: reference value (benchmark), historical activity level, exchange factor, carbon leakage and a correction factor.

Each of these factors refers to a specific point of analysis. The benchmark value is based on the average emission levels of 10% of the most efficient installations in the sector. The level of historical activity indicates the most common value of production for a given reactor. The exchange factor is determined by taking into account whether the process fuel or energy is

convertible to produce heat or mechanical energy to produce an equivalent product. Any sector that faces a significant risk of carbon leakage from exposure to non-EU competition due to price on CO_2, will receive up to 100% in this factor. Finally, the correction factor is an instrument that ensures that the total allocation remains less than the maximum limit quantity.

Based on these surveys of installed capacities, free allocations and verified emission analyzes, it was possible to carry out a diagnosis of Europe's steel mills regarding their GHG balance.

2.2. Methodology

In order to provide a better understanding of the data collected, the work was divided into four different topics: (i) GHG policies around the world; (ii) ETS context and current stage; (iii) Case study of some steel mills in Europe; and (iv) Future prospects for the industry.

The search for bibliographic references that supported this study was wide and included academic works from journals in the Engineering area, presentations from technical seminars and congresses, as well as web pages of governmental and institutional parties related to the GHG and steel industry.

Concerning the choice of the steel mills presented in this work, the following criteria were taken into account: (i) aspects of location; (ii) owner group; and (iii) mill capacity in terms of hot metal production. The objective was to select companies that could represent the diversity that exists in the European steel sector.

With regards to the technologies that were discussed here, it was highlighted those that have a more promising degree of technical potential and that contribute more significantly to the reduction of GHG.

2.3. Results and Discussion

2.3.1 Case Study of Steel Mills in Europe

In this section, a series of information was gathered from four steel mills in Europe from the following countries: Netherlands, Austria, Germany and France. The study data were consulted through the EU Transaction Log website[10], reports from the Companies and information from the Power Plants linked to the steel companies. The queries on the EU Transaction Log website were made in 2019 and focused on the OHA (Operator Holding

Accounts). This dataset consists of data on all installations covered by the EU ETS at the time of download, including the operator, ETS main activity and compliance status such as allocated allowances, verified emissions and surrendered allowances. Three types of facilities were considered for the analysis: (i) the steelmaking mill itself, (ii) the own power plants and (iii) third party power plants linked with steel mill. Distant installations such as minimills or other offsite facilities were not considered.

2.3.1.1 Dutch steel mill

The Dutch steel mill is located on the North Sea Coast of Netherlands and mainly produces flat products based on BOF route. The plant comprises of 2 coke batteries, 1 pelletizing plant, 1 sinter plant, 3 blast furnaces, 1 basic oxygen shop, 1 hot strip mill and thin strip caster, cold rolling mill, 3 galvanized lines, 1 pre-finished steel line, hot pickling, annealing and tinning lines. The steel production of this plant in 2018 was 6.9 Mt[11]. In Figures 2.1 and 2.2, it is possible to see the emission flowchart of this plant and the comparison between the verified emissions and the free license. Based on total CO_2 emissions related to this mill in EU Transaction Log and steel production published, it can be estimated that the specific emission is around 1.80 tCO_2/t steel.

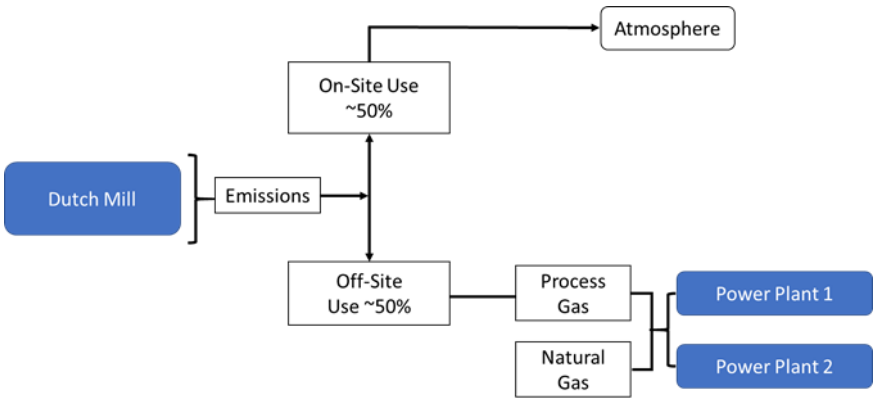

Figure 2.1: Emission distribution flow in the chain associated with the Dutch steelmaker.

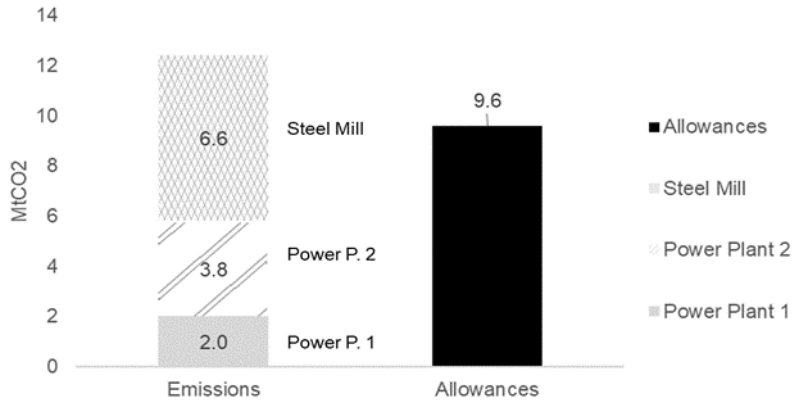

Figure 2.2: Balance between verified emissions and licenses for the Dutch steelmaker.

It is noted that half of the emissions produced at the Dutch plant are burnt to heat the furnaces within the steelmaking site, while the other half is sent to two third-party power plants. The blast furnace gas that is sent to these third-party plants creates practically the same amount of energy that is consumed in the steel operation. Another interesting point is that the isolated emission from the steel plant is less than the emission license. However, when added to the power plants emissions that should be considered in the whole balance of the steel operation license, the situation changes and there is a deficit in the carbon allowances.

2.3.1.2 Austrian steel mill

This is an integrated steel plant located in the northern part of Austria, at the Danube river. The plant has 3 blast furnaces which produce steel used for flat products for the energy sector and mechanical engineering applications. Its main products are heavy plate, hot-rolled strip, cold-rolled strip, hot-dip galvanized steel strip, electrogalvanized steel strip and organic-coated steel strip.

In 2018, this mill reported 4.62 Mt of steel production[12]. Comparing this number with the total emissions in the mill showed in Figure 2.3 it can be stated that each ton of steel produced in generated the equivalent of 1.69 tCO_2.

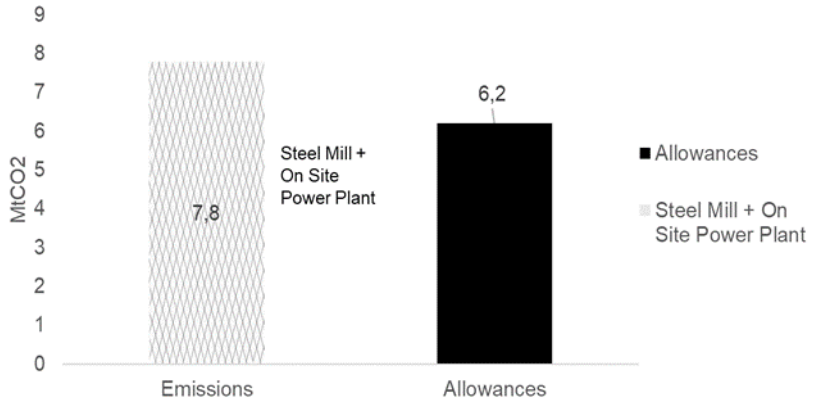

Figure 2.3: Balance between verified emissions and licenses for the Austrian steelmaker.

The Austrian power plant is integrated with the steel plant. Since 2013, this company started to report data from the power plant implicitly within the steelmaker's data, so there is no way to track the numbers separately. However, it is known that 80% of the steelmaker's energy demand is provided by this plant, the remaining is purchased on the market. It is noted that the emissions from this plant also exceed the licenses granted to the company.

2.3.1.3 German steel mill

This mill is located at the Ruhr Valley in Germany. Its products mix includes HRC, CRC, hot dipped/electrogalvanized coil, tinplate, color coated coil, electrical steel and heavy plate. Four blast furnaces operate in this site, which produced 9.8 Mt of pig iron in 2018. The steel production reached 10.4 Mt[13] and the CO_2 intensity were about 1.79 tCO_2/t steel, considering the CO_2 emitted value in Figure 2.4. Figure 2.5 shows the plant's emissions diagram as well.

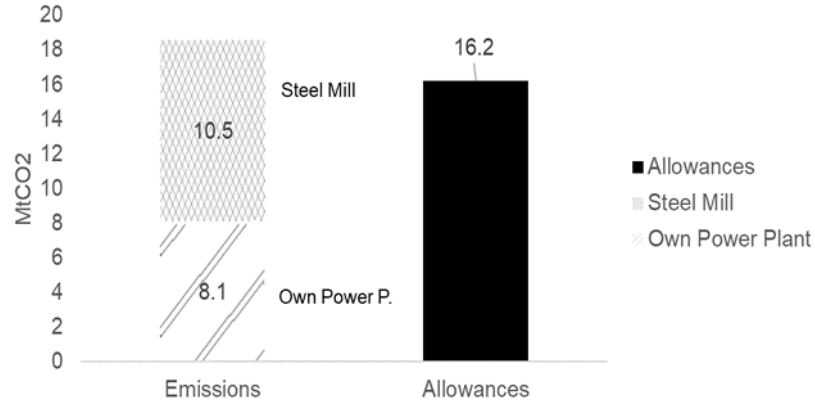

Figure 2.4: Balance between verified emissions and licenses for the German steelmaker.

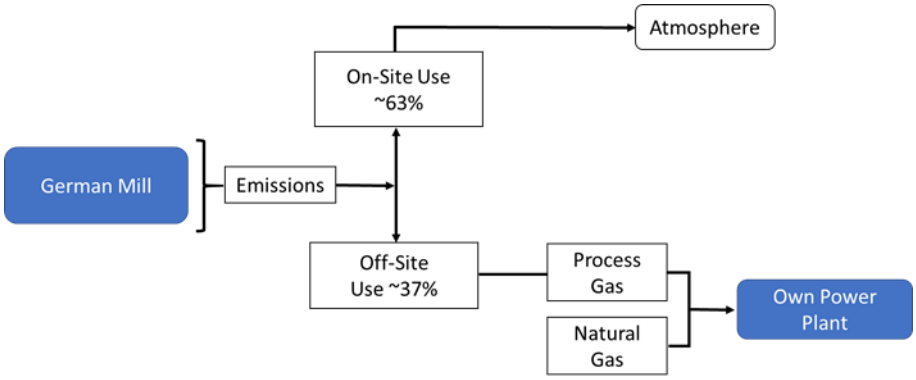

Figure 2.5: Emission distribution flow in the chain associated with the German steelmaker.

The power plant in the context is owned by the same owners as the steelmaker, but the plant is not integrated into the site as in the Austrian case. The power plant is supplied with a combination of gases where 87% comes from the top gas in the blast furnaces, 9% is CO from the coke plants and 4% comes from external natural gas. The energy generated at the power plant is preferably sent to supply the steel mill, but there is flexibility to feed the municipal domestic network. In this scenario, it can be seen that steel mill emission only is lower than the free allocation, but when adding the value of the emissions from the power plant the balance turns to shortage.

2.3.1.3 French steel mill

The French mill belongs to a big multinational steelmaking group. The plant has three blast furnaces and one basic oxygen shop. The company produces both semi-finished and finished products in the form of slabs and HRC. The main niche of customers of the plant is the automobile sector. The steel production of this unit was 6.8 Mt in 2018, with a consequent specific emission level of 1.85 tCO_2/t steel[14]. Figures 2.6 and 2.7 show information regarding the emissions flow and the balance of emissions with licenses.

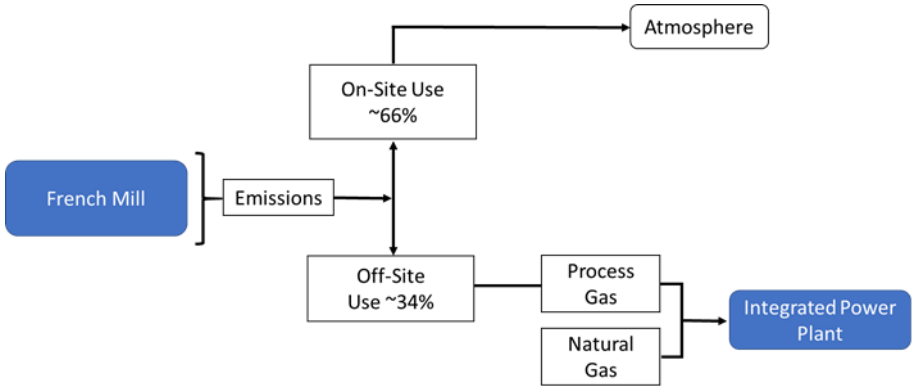

Figure 2.6: Emission distribution flow in the chain associated with the French steelmaker.

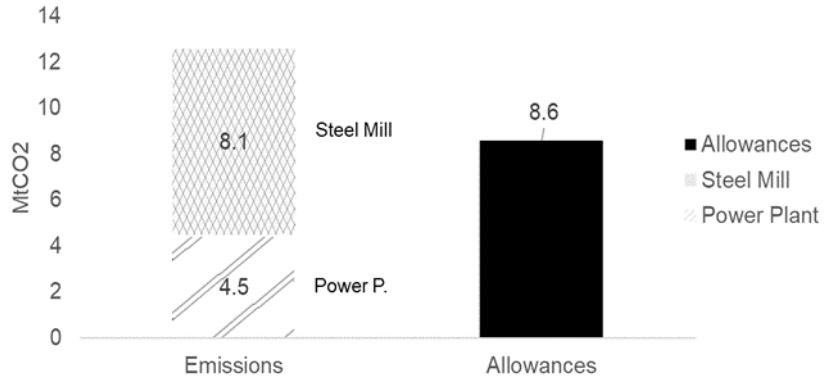

Figure 2.7: Balance between verified emissions and licenses for the French steelmaker.

Approximately two-thirds of the process gases generated from the steel mill's reactors are emitted to the atmosphere, after the usage in heating purposes and flue gases on site. On the other hand, one-third is destined for a third power plant connected to the plant. This power plant is adapted to operate with both process gas and direct supply of natural gas. The role of the electric power is to supply exclusively the operations of the steel plant and according to the data from the EU Transactions Log, the emission of the plant is 4.5 $MtCO_2$. Therefore, the total number of emissions related to the steelmaker's operation totals 12.6 $MtCO_2$ and is the largest deficit among the plants presented.

In Figure 2.8, it is possible to observe an overview of the four plants studied, where it is noted that the Austrian plant is the one that has the smallest deficit between licenses granted and emissions accounted for, besides it is also the plant with the lowest ratio of CO_2 emissions for each ton of steel produced. One of the reasons that explains the good specific emission ratio is the low coke rate of its blast furnaces, which can be explained by the use of pre-metallized burden (HBI). On the other hand, the situation of the Dutch plant and the German plant is quite similar. Both have the CO_2 intensity about to 1.8 and the emission deficit are very close. Finally, the French mill is the one with a slightly higher emission per ton of steel and also has a larger total deficit, probably due to low energy efficiency.

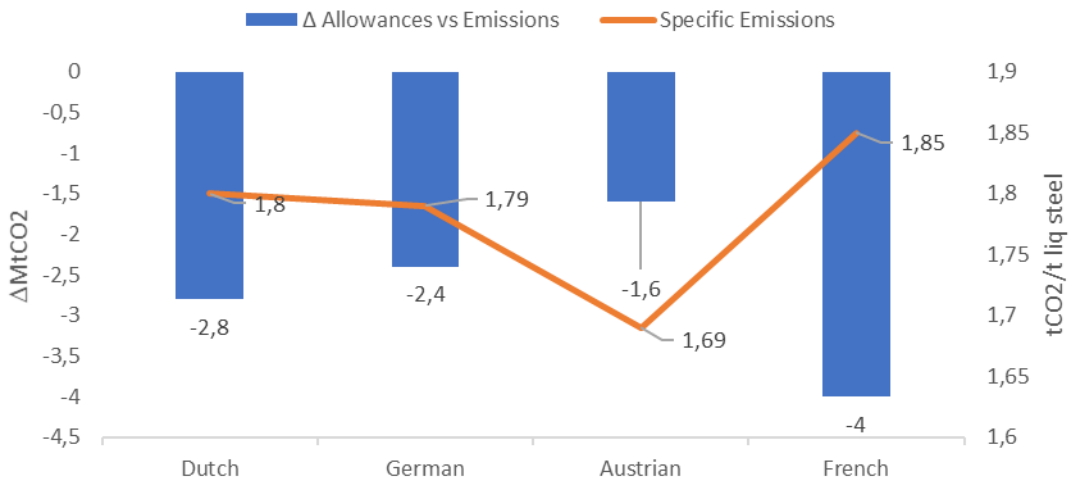

Figure 2.8: Comparison of the balance of emissions and emission efficiency per ton of steel produced.

The negative balance between emission and licenses of these four plants is an indicator of shortage, but does not necessarily imply that these steelmakers are paying penalties, since there may be mitigating alternatives:

- Savings: credits not used in previous years could have been applied in 2018 instead of paying.
- Traded: allowances through the course of the year.
- Transferred: free allowances from other plants owned by them and used to compensate for these specific mills.

2.3.2 Future trends for the steelmaking industry

Taking global aspect of the need to reduce greenhouse gases and the contribution made by industrial activity, especially in the steel chain, there is a clear need to seek technological alternatives for the primary iron routes. Most of the ongoing efforts can be divided into three different groups[15]:

- CDA (Carbon Direct Avoidance): directly avoids CO_2 emissions, either through an increase in the use of renewable energy in the manufacture of steelmaking or replacing carbon in reduction processes.
- CCU (Carbon Capture and Usage): it consists of capturing CO_2 from the industrial process and reusing it as a raw material for chemical conversion or other usages.

- CCS (Carbon Capture and Storage): it is based on the generation of a clean and concentrated CO_2 gas that can be transported and then stored.

In this context, it can be said that CCU and CCS are palliative resources and due to it they normally do not tend to generate a significant influence to solve the environmental problem. On the other hand, CDA related initiatives are naturally more disruptive and have a such greater potential impact. Among the various CDA initiatives currently being studied for the steel industry, some are highlighted:

- Routes alternatives to obtain primary iron (e.g. greater use of the DR/EAF and electrolysis).
- Use of metallic or pre-metallic in the existing routes.
- Use of less polluting fuels (e.g. biomass).
- Use of cold agglomerates as burden.
- Use of electrolysis process.
- Greater use of hydrogen as a reducing agent in processes.

According to the WSA (2018), the BF/BOF route usually emits approximately 1.85 tons of CO_2 per ton of steel produced, whereas 1 ton of steel via the DR-EAF route is responsible for 0.81 tons of CO_2[6]. Factors such as the chemical quality of raw materials loaded in the furnace and the scrap proportion play an important role on the numbers commented by the WSA. However, when comparing the two main technically and economically feasible routes for obtaining steel in the world, it is observed that there is already an important difference on the emissions related to routes. Basically, the direct reduction route has a considerable use of hydrogen that transforms into water steam and then is reformed with natural gas. However, what still limits the expansion of the use of the DR route in many places, remains the low availability of low-cost natural gas[16]. Middle East and North Africa are historical regions with abundant natural gas reserves, but more recently other countries as US have increased its production of sponge iron due to the exploitation of new reserves[17].

Some companies already have plans to partially or gradually replace their current routes to direct reduction and electric furnace routes. Salzgitter, for example, has the SALCOS® project (Salzgitter Low CO_2 Steelmaking) which aims to produce steel with a flexible and increasing use of H_2[18]. To achieve this goal, they signed a partnership with Tenova to install the ENERGIRON-ZR reactor combined with a CO_2 capture equipment. The expected result is that with this route replacing the blast furnace there will be a 95% reduction in CO_2 emissions[19].

In those circumstances of higher usage of DR route, the HYBRIT project (Hydrogen Breakthrough Ironmaking Technology) led by three Swedish companies, LKAB (supplier of ore and pellets), SSAB (steel mill) and Vattenfall (energy utilities) stands out. This project started in 2016 and more recently in 2018 the proof of concept was completed[20]. The goal is to drastically reduce CO_2 emissions from ironmaking, eliminating the need of fossil fuel to reduce ore.

The engineering of this technology initially consists of electrolysis cells that produce H_2 and O_2 from water. Then the H_2 is stored and before entering the DR reactor, it passes through a condenser. Inside the shaft it promotes the reduction of the iron oxides present in the burden and at the upside section the top gases are collected and redirected to the condenser circuit, where the water vapor is collected and again submitted to the electrolysis cells. Although many of the components of HYBRIT are already well-known, there are still some challenges such as process integration, product quality (raw material needs), H_2 production and storage technology, steel mill integration with power station supported by renewable sources and low percentage of carbon (cementite) in sponge iron, which impacts electric consumption in EAF[21]. From an economic point of view, it is estimated that the cost of the steel produced in HYBRIT will be 20 to 30% larger than steel produced on a conventional route. The feasibility of this new route is highly dependent on the green hydrogen production capacity and its associated costs in the future.

Another interesting development, even more disruptive, because it is a completely new reduction technology, is the project carried out between partners in Austria (VoestAlpine, University, K1-Met) called SuSteel (Sustainable Steel). The reactor consists of a conical reactor with refractory lining and a cylindrical upper part with a water-cooling system. While fines from ores and additives are loaded through the hollow electrode, argon or nitrogen are used as plasma gas and hydrogen as a reducing agent. Thus, the fed material is pushed directly into the plasma arc zone, where reduction and melting occur very quickly. The gas flow takes care of transporting the materials through the tubes and a mass spectrometer measures the composition of the gas during the test. The process works in a batch model and at the end of the operation, the liquid iron solidifies in the reactor and after decoupling the electrode, the solid metal solution is discharged by a crane[12].

Since most of these projects and initiatives for the development of new routes and/or intensive use of hydrogen in Europe are medium and long term, there are other actions that are being evaluated for the short term[22]. Such actions include the injection of H_2 into conventional

blast furnaces. The rates that have been tested are low due to operational restrictions and caution that must be taken, for example with the thermal balance. However, the environmental impact is already well known. A recent study[23] showed that under regular operating conditions a hydrogen injection of 27.5 kg/t hot metal can reduce relative emissions by 21.4 % when compared to a typical operation using pulverized coal at a rate of 120 kg/t hot metal.

Finally, the promising higher use of hydrogen in the steelmaking chain leads to a major challenge to generate H_2 with technical, environmental and economic sustainability, and competitiveness. The most common route to obtain hydrogen today is through gas reform reactions that originally consume natural gas as the main input[24,25]. Other cleaner ways, such as using biomass combined with CO_2 capture and, as a state of the art, using water electrolysis with related renewable energy source, are the target of many projects, but persist with the production cost as main obstacle[26].

2.4.Conclusions

In view of the study presented, it can be concluded that:

- The demand for greener products and more sustainable processes in the steelmaking industry will be increasing. In Europe, a region where the ETS is well established, the impact of these policies on the steel industry is notable. Four plants from different countries faced a deficit between the allowances and the verified emissions. In addition, it is also interesting to note that the efficiency of emissions per ton of steel produced varied in minor quantities from one plant to another.
- Among the existing approaches to prevent GHG emissions, the CDA causes the most positive impact and, therefore, it has guided several projects of new technological routes. Most of the new low-carbon technological routes go through intensive use of hydrogen as a reducing agent. Existing projects at different maturity degrees, ranging from the migration from conventional BF/BOF route to DR routes, to new equipment and routes and the use of hydrogen in conventional blast furnaces.
- Hydrogen production is a critical factor both for calculating the carbon footprint and for the associated costs. Electrolyzers powered by wind, solar or nuclear generators would be the most environmentally friendly paths.

- Fossil-free steel will certainly be more expensive than current steel production. Assessing market segments that are willing to pay a premium for green steel products is an important point for discussing projects.
- Studies on sustainable steel production alternatives need to be further explored and disseminated. In a global and ubiquitous industry such as steelmaking, those who focus efforts in this line and succeed, will certainly acquire competitive advantages that may be decisive in the future.

Conflicts of interest

The authors declare no conflicts of interest.

Acknowledgments

The authors would like to thank CAPES-PROEX, FAPEMIG and CNPQ, as well as all collaborators involved in the work at Vale S.A. and Federal University of Minas Gerais (UFMG).

References

[1] Mathiesen L, Maestad O. Climate policy and the steel industry: achieving global emission reductions by an incomplete climate agreement. The Energy Journal, 2004; v.25, n.4.

[2] United Nations Climate Change. The Paris Agreement [online]. 2017. [accessed 20.05.2020]. Available in: https://unfccc.int/process-and-meetings/the-paris-agreement/the-paris-agreement.

[3] Wadhwa D, Mani MS, Hussein Z, Gopalakrishnan BN. Paris Climate Agreement and the Global Economy, 2018.

[4] Change OC. World Meteorological Organization. Intergovernmental panel on climate change, 2007.

[5] EU Commission. EU ETS Handbook. Brussels, Belgium, 2015. Available in: https://ec.europa.eu/clima/sites/clima/files/docs/ets_handbook_en. pdf.

[6] World Steel Association. Steel's Contribution To A Low Carbon Future And Climate Resilient Societies [online], 2018, [accessed 20.05.2020]. Available in:

https://www.worldsteel.org/en/dam/jcr:7ec64bc1-c51c-439b-84b8-94496686b8c6/Position_paper_climate_2020_vfinal.pdf.

[7] International Carbon Action Partnership. Emissions Trading Worldwide: Status Report 2018. 2018.

[8] International Carbon Action Partnership. ETS Map [online]. 2019. [accessed 20.05.2020]. Available in: https://icapcarbonaction.com/en/ets-map?etsid=79.

[9] Borghesi S, Montini M, Barreca A. The EU ETS: The Pioneer - Main Purpose, Structure and Features. In: The European Emission Trading System and Its Followers. Springer, Cham, 2016; p. 1-28.

[10] E U Community Independent Transaction Log. Emission Trading System (EU ETS) [online]. Climate change, Environment, European Commission, 2018, [accessed 05.10.2019].

[11] EUROPE, Tata Steel. Sustainability Report FY 18-19 [online], 2019. [accessed 20.05.2020]. Available in: https://www.sabprofiel.com/assets/user/Documentatie/Tata%20Steel%20Sustainability%20Report%20FY18-19_English.pdf.

[12] Voestalpine, Group. 2019 Enviromental Statement [online], 2019. [accessed 20.05.2020]. Available in: https://www.voestalpine.com/group/static/sites/group/.downloads/en/group/2019-environmental-statement.pdf.

[13] Thyssenkrupp, Group. Lagebericht 2018-2019 Master [online], 2019. [accessed 20.05.2020]. Available in: https://ucpcdn.thyssenkrupp.com/_legacy/UCPthyssenkruppAG/assets.files/media/investoren/berichterstattung-publikationen/update-21.11.2019/en/thyssenkrupp-gb-2018-2019-en-web_neu.pdf.

[14] ArcelorMittal, Group. AM Factbook 2018 [online], 2019. [accessed 20.05.2020]. Available in: https://factbook2018.arcelormittal.com/~/media/Files/A/Arcelormittal-Factbook-2018/AM_FactBook_2018.pdf.

[15] Sormann A, Seftejani MN, Schenk J, Spreitzer D. Hydrogen-The Way to a Carbon free Steelmaking, AdMet2018.

[16] Smil V. Still the iron age: iron and steel in the modern world. Butterworth-Heinemann, 2016.

[17] Arens M, Worrell E, Eichhammer W, Hasanbeigi A, Zhang Q. Pathways to a low-carbon iron and steel industry in the medium-term- the case of Germany. Journal of cleaner production, 2017; 163. (p. 84-98).

[18] Hille V, Redenius A. SALCOS–schrittweise, flexible Dekarbonisierung auf basis bewährter Technologie. Stahl Eisen,02018; v.138, n.11, (p. 95-101).

[19] Dorndorf M, Duarte P, Argenta P, Maggiolino S, Marcozzi M. Transforming the steelmaking process. Steel Times International, 2018; v.42, n.7, (p. 29-32).

[20] HYBRIT. - Fossil-Free Steel: Summary of Findings from HYBRIT Pre-Feasibility Study 2016–2017 [online], 2018, [accessed 20.05.2020]. Available in: https://ssabwebsitecdn.azureedge.net/-/media/hybrit/files/hybrit_brochure.pdf.

[21] Åhman M, Olsson O, Vogl V, Nyqvist B, Maltais A, Nilsson LJ, et al. Hydrogen steelmaking for a low-carbon economy. Stockholm: Stockholm Environment Centre and Lund University, 2018.

[22] Warner NA. Zero CO2 steelmaking in a future low carbon economy. 1. Energy conservation in smelting hematite ore directly to refined iron slab. Mineral Processing and Extractive Metallurgy, 2018; v.127, n.2, (p. 73-83).

[23] Yilmaz C, Wendelstorf J, Turek T. Modeling and simulation of hydrogen injection into a blast furnace to reduce carbon dioxide emissions. Journal of Cleaner Production, 2017; v.154, (p. 488-501).

[24] Tacke KH, Steffen R. Hydrogen as a reductant for iron ores and the effects on CO2 formation. In: Proceedings of International Symposium on Global Environment and Steel Industry (ISES'03), 2003.

[25] Mosca L, Jimenez JAM, Solomon AW, Gallucci F, Palo E, Colozzi M, et al. Process design for green hydrogen production. International Journal of Hydrogen Energy, 2020; v.45, n.12, (p. 7266-7277).

[26] NOLDIN, J. Decarbonization and Green Eletricity in the Steel Industry [online]. ABM Magazine, v. 655, (p. 22-32) [accessed 16.06.2020]. Available in: https://revistaabmdigital.com.br/edicoes/655/#p=22.

Capítulo 3. Artigo B - Evaluation of the impact of cluster formation in a direct reduction shaft furnace through numerical simulation

Jean Philippe Santos Gherardi de Alencar [a,*], *Bruno Amaral Pereira*[b], *José Adilson de Castro*[c], *Valdirene Gonzaga de Resende* [a] *and Wander Luiz Vasconcelos*[d]

[a]Marketing Department, Vale S.A., Nova Lima, MG, Brazil
[b]Bruno A Pereira Consultoria, Resende, RJ, Brazil
[c]Metallurgical Department, Fluminense Federal University, Volta Redonda, RJ, Brazil
[d] Metallurgical Department, Federal University of Minas Gerais (UFMG), Belo Horizonte, MG, Brazil

* Corresponding author
Email: jeanpga@gmail.com

Artigo submetido a Revista Escola de Minas Review Código de submissão: REMI-2021-0037
Received: 17 May 2021 - Accepted: 9 July 2021
REM, Int. Eng. J., 74(4), 451-461, 2021
https://doi.org/10.1590/0370-44672021740037

ABSTRACT

The Direct Reduction (DR) process has been growing worldwide, and there are strong context suggestions that it will grow even more. One of these factors is the environmental pressure that occurs worldwide, and there are already projects to migrate Blast Furnace route steel plants to the Direct Reduction (DR) route, due to its smaller carbon footprint. Considering the importance of this process and the challenges of carrying out experimental tests on a pilot scale, an adequate way to evaluate the process and its impacts is through numerical simulations. There are different techniques applied to models that describe the counter-current reactor in the DR process, but none of them account for the clustering phenomenon. Clustering occurs because of the sintering of the metallic iron on the surface of the pellets in such a way that they attach to each other, forming clusters that hinder the gas flow through the shaft. The present study attempted to adapt a numerical model of a DR process to account for the effect of the cluster

formation. Some clustering index equations from literature and some developed as part of this study were used and tested in the model, as a function of temperature, by varying the solid volume fraction in the control unit. The equation that resulted in the adjusted output closest to the current empirical value was implemented in the model and proved to be successful.

Keywords: iron ore, direct reduction, simulation, clustering.

3.1.Introduction

DRI (direct reduced iron) production in 2019 reached 108.1 Mt, representing an increase of 7.3% compared to the year 2018. It was the fourth consecutive year of increase. More than 75% of this DRI production comes from a reduction process in shaft furnaces (Midrex, 2020). Some countries such as India, Iran, Algeria, USA and Russia have stood out in this scenario due to new projects and plant reconditioning. In addition, the need for technologies with lower greenhouse gas emissions is a relevant driver for new investments in the future. It is estimated that a DR route with a 100% H_2 atmosphere may reduce emissions by approximately 80% compared to a conventional Blast Furnace route (Costa et al., 2013, Arens et al., 2017, Hille, 2018, Ahman et al., 2018, Dorndorf, 2018, HYBRIT, 2018). However, the process has some challenges in its operation to guarantee dynamic process control and product quality. One of the challenges is the sintering of metallic iron formed at high temperatures and the associated reducing atmosphere causing the formation of clusters (Zhang et al, 2012, Yi et al, 2013, Battle, 2014, Alencar, 2016).This condition comes from when some raw material with a high susceptibility for sticking enters the shaft furnace. So, an increase in the bed pressure is noted, which tends to increase gradually.

The reduction process that takes place inside a direct reduction reactor is complex, as it involves a set of thermochemical reactions in a heterogeneous phase system. In this context, a huge number of models have already been developed trying to represent the DR process. These models range from single-particle approaches to multiparticle and components models with topochemical and grain models (Venkateswaran and Brimacombe, 1977, Yu and Gillis, 1981, Takenaka and Kimura, 1986, Negri, 1991 and 1995, Parisi and Laborde, 2004, Piotrowski et al., 2005, , Pineau et al., 2006, Thurnhofer, 2006, Valipour et al., 2006, Ajbar et al., 2011, Nouri, 2011, Costa et al., 2013, Shams and Moazeni, 2015, Kazemi, 2017, Castro, 2018, Rocha et al., 2019). Since the DR process can be summarized as a counter-current bed composed of solid

and gas into a mass and heat transfer, the most acceptable and useful models correspond to numerical models that comprise the multi-interaction and multiple phase theory.

The insertion of elements and components that best describe the phenomena associated with the direct reduction process is a continuous target to achieve better operational predictability and quality values. A recent example that can be cited is the study of the particle shape factor charged in a Corex reactor (You et al., 2019). But there are still no models that consider the phenomenon of clustering formation impacting the bed's permeability and its stability.

In this sense, the present study used data from other studies (Pereira, 2012, Alencar, 2016, Griscom et al., 2000) concerning the clustering index in different temperatures to provide enough data to establish parameters and correlations that could be added in a model based on transport equations applied to reactive multiphase and multicomponent systems in order to estimate the impact of cluster formation inside the bed on the operational parameters.

3.2.Methodology

3.2.1. Clustering Index Experiment

The standard test to measure the susceptibility of clustering formation is the ISO11256. This test is based on an isothermal reduction at 850 °C in a reducing atmosphere composed of CO and H_2. At the end of the test, the reduced mass is weighed and put into a tumbling cycle. At the end of each revolution, the mass in the form of a cluster is weighed and subjected to the drum again (ISO, 2007). Eq.1 shows how the international standard ISO11256 standard establishes the clustering index.

$$CI = \frac{100}{8\,x\,m_r}\,x\,\sum_{i=1}^{8} cm_i \qquad (1)$$

Where:

m_r is the total mass after reduction and

cm_i is the mass (g) of the cluster portion after each revolution "i".

Previous studies (Pereira, 2012, Zhang et al., 2012, Yi et al., 2013, Alencar, 2015 and 2016) evaluated the metallic iron morphology present at different pellet clusters considering different reduction temperatures. According to these studies, as the reduction temperature increases, the clustering index also rises. Based on these data, it was possible to formulate Equations 2, 3, 4 and 5 that correlate with the clustering index (CI) as a function of temperature. Three of these

equations consider the effect of temperature as linear and one considers the effect as exponential. All of them were evaluated in this study.

$$CI1\ (\%) = 0.38 \times T(°C) - 308.67 \quad \text{(Alencar, 2015)} \quad (2)$$

$$CI2\ (\%) = 0.445 \times T\ (°C) - 376.75 \quad \text{(Alencar, 2015)} \quad (3)$$

$$CI3\ (\%) = 0.435 \times T\ (°C) - 347.25 \quad \text{(Alencar, 2015)} \quad (4)$$

$$CI4\ (\%) = 0.0004e0.0122 \times T(°C) \quad \text{(Pereira, 2012)} \quad (5)$$

3.2.2. Modeling Concept

3.2.2.1.General Conditions

The mathematical modeling of the DR process in the shaft furnace can be represented by the transport equation of momentum, energy and chemical species (Melaaen, 1992, Castro et al., 2018, Patankar, 2018, Rocha et al., 2019). In this approach, two phases can be discriminate, gas and solid. The gas phase is represented by the reductant gas injected in the reduction zone, the gas generated in the reduction reaction and reform, the cooling gas, and the carburization reaction. The solid phase is the metallic burden, that is composed of pellets and lump. The model can also represent the size distribution, divided into granulometric ranges for the pellets and lump. In this implementation, kinetic constants were assumed to be the same for all materials. Thus, the reduction rate is different due to physical characteristics, such as size, shape factor and porosity.

The principle of solid arrangement in the control volume is assumed. Thus, this approach considers that the gas phase fills the voids. Therefore, as in the rule of continuity, then Equation 6 can be applied.

$$\varepsilon_{g+}\varepsilon_{s=1} \quad (6)$$

The term ε_g in the above equation corresponds to the gas fraction and the ε_s is the solid fraction in the volume. To calculate the solid fraction in the volume, the mixture rule is applied according to Equation 7.

$$\varepsilon_{s=\sum f_m} \quad (7)$$

The granulometric ranges for pellets and lumps in the solid phase are represented by the index “m” in the above equation.

3.2.2.2. Process Governing Equations and Boundary Conditions

For each phase considered in the control volume, the conservation rule is applied. Thus the momentum, energy and chemical species transport equation can be calculated. To represent the industrial process, the corresponding boundary conditions are applied in these equations. The fluxes and volumetric composition to the reduction and cooling gas inlet are assumed to be known. For the gas phase, the reduction and cooling zone are considered. Due to pressure difference, the gas does not pass from one zone to another. The solids assume movement against the upward gas flow and it is allowed to pass through these two zones. In the wall region, the gas is non-slip, and for the interaction with the solid particles, a friction coefficient is adopted. To represent the cooling of the refractories, a heat exchange coefficient is applied to the walls. For the two phases, the flows are assumed to be completely developed at the outlet.

Equations 8 to 11 represent the phase momentum, mass conservation, energy, and chemical species, respectively.

$$\frac{\partial(\rho_i \varepsilon_i u_i)}{\partial t} + div\left(\rho_i\, \varepsilon_i\, \vec{U}_i\, u_j\right) = div\left(\varepsilon_i \mu_i grad\left(u_j\right)\right) - grad(\varepsilon_i P_i) - F_i^k \qquad (8)$$

$$\frac{\partial(\rho_i \varepsilon_i)}{\partial t} + div\left(\rho_i\, \varepsilon_i\, \vec{U}_i\, \right) = \sum_{n=1}^{nreacts} R_n^i \quad (9)$$

$$\frac{\partial(\rho_i \varepsilon_i h_i)}{\partial t} + div\left(\rho_i\, \varepsilon_i\, \vec{U}_i\, h_j\right) = div\left(\frac{k_i}{c_{p_i}}\left(h_j\right)\right) + \sum_{n=1}^{nreacts} R_n^i\, \Delta h_n^i + E_i \qquad (10)$$

$$\frac{\partial(\rho_i \varepsilon_i \varphi_i)}{\partial t} + div\left(\rho_i\, \varepsilon_i\, \vec{U}_i\, \varphi_{i,specie}\right) = div\left(\varepsilon_i D_{specie}^{bulk} grad\left(\varphi_{i,specie}\right)\right) + \sum_{n=1}^{nreacts} M_{specie} R_n^i \qquad (11)$$

In the above equations, the index *i* and *j* represent the phases and velocity components, and n represents the chemical reactions. The terms μ, ε, ρ are the dynamic viscosity volumetric fractions and phase densities, respectively. *U* and *u* are vectors and velocity components. *P* is the pressure and *F* are the exerted strength by other phases. *Cp*, *k* and ΔH are heat capacity, thermal conductivity and heat due to chemical reactions, respectively. *R* is the reaction rates and *M* is the molecular weight of the species.

3.2.2.3.Phase Interactions

Regarding phase interactions, the model considers the momentum, energy and mass changes. The momentum interactions are modeled by semi-empirical equations (Eq. 12 and 13) with adjusted constants to the shaft furnace process.

Momentum interaction:

$$F_g^s = -F_s^g = [\sum_m f_m F_m]\left|\vec{U}_g - \vec{U}_s\right|\left(u_g - u_s\right) \quad (12)$$

$$F_m = 150\mu_g \frac{1}{|\vec{U}_g - \vec{U}_s|}\left(\frac{\varepsilon_m}{(1-\varepsilon_m)d_m\varphi_m}\right)^2 + 1.75\rho_g\left(\frac{\varepsilon_m}{(1-\varepsilon_m)d_m\varphi_m}\right) \quad (13)$$

The indexes *g* and *s* indicate gas and solid respectively, m is the granulometric range of the solid phase component, *f* is the volume fraction of the granulometric range of the component in the solid phase, *F* is the interaction strength between the phases, *d* is the mean diameter of the granulometric range of the component in the solid phase and φ is the mean shape factor in the granulometric range of the component in the solid phase.

3.2.2.4.Convection and radiation energy transfer

Equation 14 is applied to modeling the heat transfer between the solid phase components and the gas phase.

$$E_g^s = -E_s^g = \frac{6\varepsilon_m}{d_m\varphi_m}\frac{k_g}{d_m\varphi_m}\left[2 + 0.39\left(\frac{\rho|U_g|}{\mu_g}(d_m\varphi_m)\right)^{\frac{1}{2}}\left(\frac{\mu_g C_{pg}}{k_g}\right)^{\frac{1}{3}}\right]\left(T_g - T_m\right) \quad (14)$$

The above equation is accountable for convective and radiation heat transfer among the phases and *T* is the phase temperature.

3.2.2.5.Phase Properties

Based on its components, the mixing rule is used to calculate the solid and gaseous phase properties. From the ideal gas law, we can determine the gas-phase density.

$$\rho_g = \frac{P_g}{RT_g}\sum \emptyset_{j,g} M_j \quad (15)$$

In the above equation, the subscript *j* means the gas species. The viscosities of these components are determined as follows (Bird et al., 1960, Reid et al., 1988).

$$\mu_g = 2.6693 \times 10^{-6}\frac{1}{\Omega_{\mu,j}}\sqrt{\frac{M_j T_g}{\sigma_j}} \quad (16)$$

The terms that appear in the equation are presented below:

$$\Omega_{\mu,j} = \frac{1.16145}{(T^*)^{0.14874}} + \frac{0.52487}{exp(0.77320T^*)} + \frac{0.52487}{exp(2.43787T^*)} \quad (17)$$

$$T^* = \frac{K_{Boltzmann}T_g}{\epsilon_j} \quad (18)$$

The Eucken´s polyatomic gas approximation is used to determine the thermal conductivities for the components (Wilke, 1950, Neufeld et al., 1972).

$$K_j = M_j\left(C_{p,j} + \frac{5R}{4M_j}\right) \quad (19)$$

The wilke method (Wilke, 1950) is used to determine the viscosity and thermal code of the phase.

$$\lambda_g = \sum_{j\epsilon g}\left[\frac{\gamma_{j,g}\lambda_j}{\sum_{jj\epsilon g}\left(\gamma_{jj,g}\chi_{j,jj}\right)}\right] (\lambda = \mu, k) \quad (20)$$

$$\gamma_{j,g} = \frac{(\emptyset_{j,g}/M_j)}{\sum_{jj\epsilon g}(\emptyset_{jj,g}/M_j)} \quad (21)$$

$$\chi_{j,jj} = \left\{1 + \left(\lambda_j/\lambda_{jj}\right)\left(M_{jj}/M_j\right)^{1/4}\right\}^2 \quad (22)$$

Where it is possible to determine the binary diffusivity of the gas species according to the equation below.

$$D_{j,k}^T = 0.0018583\ X\ 10^{-4}\frac{T^{1/2}\sqrt{\left(\frac{1}{M_j}\right)+\left(\frac{1}{M_k}\right)}}{(P_g/101325)\sigma_{ave}^2\Omega_{ave}} \quad (23)$$

The terms of the above equation are determined as follows:

$$\sigma_{ave} = 0.5\left(\sigma_j + \sigma_k\right) \quad (24)$$

$$\Omega_{ave} = \frac{1.06036}{(T^*)^{0.15610}} + \frac{0.19300}{exp(0.47635T^*)} + \frac{1.03587}{exp(1.5299T^*)} + \frac{1.76474}{exp(3.89411T^*)} \quad (25)$$

$$T^* = \frac{K_{Boltzmann}T_g}{\epsilon_{ave}} \quad (26)$$

$$\epsilon_{ave} = \sqrt{\epsilon_j\epsilon_k} \quad (27)$$

The above terms are: Boltzmann constant and σ and ∈ which are related to the collision gas types (Bird et al., 1960, Reid et al., 1988).

The equation below defines the gas temperature as a function of gas composition and enthalpy.

$$H_g = \sum_{j\in g} \emptyset_{j,g} \left[\Delta H_{j,g}^{298k} + \int_{298k}^{Tg} C_{p,j}(T)dT\right] \quad (28)$$

$$C_{p,j}(T) = a_j + b_j T + c_j T^{-2} \quad (29)$$

Based on the solid properties, the component's heat capacity are calculated as a function of temperature.

$$C_{p,k} = a_k + b_k + T_s + \frac{c_k}{T_s^2} \quad (30)$$

$$C_{P,s} = \sum_{k\in s} C_{p,k}\emptyset_{k,s} \quad (31)$$

$$H_s = \sum_{k\in s} \emptyset_k \left[\Delta H_k^{298k} + \int_{298k}^{T_s} C_{p,k}(T)dT\right] \quad (32)$$

Considering the intra-bed radiation and the limit layer convection, the thermal conductivity is determined (Bird et al., 1960, Reid et al., 1988, Akiyama et al., 1992).

$$K_{s,eff} = (1-\varepsilon_s)\left(k_g + a\right) + \varepsilon_s \left[\frac{2}{k_s} + \left(\frac{k_g}{0.274} + b\right)^{-1}\right]^{-1} \quad (33)$$

The term es is the emissivity of solid components and the above constants are determined as follows:

$$a = \alpha \left[1 + \left(\frac{1-\varepsilon_s}{\varepsilon_s}\right)\left(\frac{1-\mathrm{e}_s}{\mathrm{e}_s}\right)\right]^{-1} \quad (34)$$

$$b = \alpha \left(\frac{\mathrm{e}_s}{2-\mathrm{e}_s}\right) \quad (35)$$

$$\alpha = 0.1952 d_s \left(\frac{T_s}{100}\right)^3 \left(\frac{4.184}{3600}\right) \quad (36)$$

3.2.2.6.Numerical Solution

The model uses the finite volume method (FVM) to discretize the equation of mass, energy, momentum and species taking into account a general coordinate system (Piotrowski et al., 2005, Pineau et al., 2006). These equations are integrated over a controlled volume; thus, a set of algebraic equations is created. The power-law scheme is used to determine the algebraic equation coefficients (Pineau et al., 2006). To improve the coupling of the pressure and velocity fields, the SIMPLE algorithm technique is used iteratively. To efficiently solve the algebraic equation system, the tridiagonal matrix algorithm based on the line by line solution is used. To

improve the convergence, the alternated direction implicit is applied in the model solver. The solution is obtained iteratively to a stationary condition. The solution accuracy is reached by convergence criteria of 10^{-6} for the energy and momentum equation. The convergence target to the mass balance equation considers a difference of 0.01.

3.2.3. Pellets Clustering Modeling

Taking into account the tests and results mentioned above where it is possible to obtain a correlation between temperature and clustering index, the model applied the equations to consider the presence of pellet clusters inside the DR reactor.

All equations formulated were applied in the model considering the increase of the solid fraction in the control volume and consequently decreasing the gas permeability to the region. In order to increase the solid volume fraction, the mean diameter dm of each solid component is recalculated as a function of *CI* (Eq. 37), where *CI* is the Clustering Index in decimal format.

$$d_m' = d_m * (1 - CI) \quad (37)$$

The empirical equations (Parisi and Laborde, 2004) for the solid fraction component ε_m are actualized according to the new diameter in Equation 38:

$$\varepsilon_m = 1 - 0.403[100 d_m]^{0.14} \quad (38)$$

The sum of solid fraction components is used to determine the gas volume fraction (Eq. 39).

$$\varepsilon_s = 1 - \sum \varepsilon_m \quad (39)$$

Figure 3.1 schematically shows the configuration of the control volumes in different aspects. Scenario A shows a reference situation with the pellets' average diameter (d_m). Scenario B demonstrates the real aspect of the pellets that, under reduction and high temperatures, faces softening, deformations, and the sticking phenomena, leading to the gas flow disturbance. On the other hand, scenario C is the representation of the approach given in the present study, where the smaller diameter of the pellets generates a greater packing factor and, consequently, greater pressure drop, resulting in the same practical effect observed in scenario B.

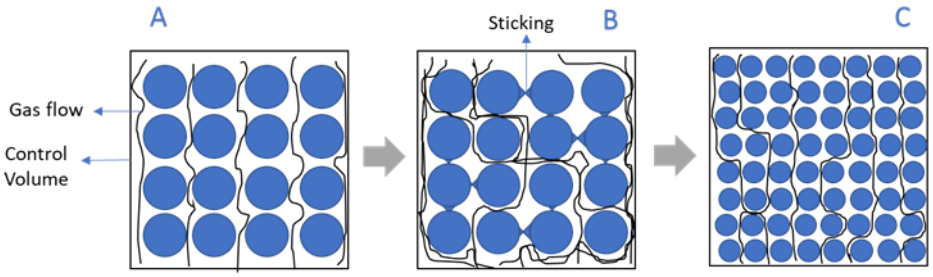

Figure 3.1 - Schematic representative diagram of the control volume: (A) condition without clustering, (B) real flow condition with clustering and (C) condition with clustering as represented in the model.

3.3.Results and Discussion

The evaluation of the clustering equations with different temperatures was validated, aiming similar results that were achieved in two industrial cases. In both scenarios, the reactor was a shaft furnace type, and the impact of the clustering index was converted into relative productivity. After comparing and defining the best prediction equation for CI and its impact on solid volume fraction, new temperature scenarios were tested to evaluate the sensibility related to it.

3.3.1. Validation of the Reference Model with Industrial Data

Before starting the tests involving the new elements in the model, such as the equation that correlates solids fraction as a function of the clustering index, an initial validation of the model was carried out based on a shaft furnace's industrial data from a mill located in MENA. Tables 3.1 and 3.2 show, respectively, the main operational data of this industrial reactor and the predominant gas composition in the reduction and cooling zones.

Table 3.1 - Industrial data from a shaft furnace reactor.

Process Parameters	
Solid temperature [ºC]	33
Reduction Gas Temperature [ºC]	985
Reduction gas Flow rate [Nm3/min]	2764
Cooling Gas Temperature [ºC]	30
Cooling Gas Flow rate [Nm3/min]	850
Number of bustle gas inlets	72
Bustle gas diameter [mm]	120

Table 3.2 - Gas composition used in the reactor and model.

Gas composition								
	N_2	O_2	CO	CO_2	H_2	H_2O	CH_4	C_2H_6
Reduction gas Composition [vol%]	3.44	0.0	28.98	2.32	53.66	6.4	4.98	0.1
Cooling gas Composition [vol%]	6.13	0.0	0.92	1.24	6.06	3.5	82.15	0.0

It can be seen in Table 3.1 that the operational practice of the selected reactor is in line with the typical modus operandi of DR plants, where the raw material pellet enters the reactor at room temperature, and the bustle gas temperature is around 1000 °C (Atsushi, 2010). In addition, Table 3.2 shows that the reduction gas composition has an H_2/CO ratio of approximately 1.85, which is a value that guarantees good conditions for reduction kinetics and thermal balance in the system (Capriotti, 2012). Finally, the cooling gas is very rich in CH_4 to favor the carburization and self-reforming process inside the reactor.

The pellet burden used in this validation step also represented the market share consumed by this mill studied. Three pellets from different suppliers were simulated according to chemical and granulometric quality highlighted in Tables 3.3 and 3.4.

Table 3.3 - Raw material chemical composition.

	FeT	FeO	SiO_2	Al_2O_3	CaO	MgO	P
Pellet A	67.72	NA	1.61	0.46	0.78	0.07	0.022
Pellet B	67.79	0.13	1.37	0.41	0.84	0.12	0.042
Pellet C	67.81	0.31	0.81	0.17	0.94	0.61	0.027

Table 3.4 - Raw material particle size distribution.

Materials		Range 1	Range 2	Range 3	Range 4	Range 5
Pellet A (50% in burden)	Size distribution (mm)	16	12.5	10.0	8	- 5
	Fraction (%)	1.6	55.4	35.5	6.5	0.2
Pellet B (10% in burden)	Size distribution (mm)	16	12.5	10.0	8	-5
	Fraction (%)	1.4	53.5	42.1	2.4	0.6
Pellet C (40% in burden)	Size distribution (mm)	16	12.5	10.0	8	-5
	Fraction (%)	2.9	36.6	51.7	2.5	0.6

According to Table 3.3, all pellets in the mix have similar iron content. However, the acid gangue content is lower in pellet C, which also has the highest values of CaO and MgO. Meanwhile pellets A and B are very similar in general, but pellet B has higher binary basicity and higher phosphorus content. In terms of size distribution, Table 3.4 presents in detail the particle size fractions of each pellet tested in the simulation. These data are one of the model inputs and are used to calculate the average particle size and consequently the bed porosity. Through Table 3.4, it is possible to say that pellet A has the distribution of larger pellets, while pellet C has the distribution of smaller pellets. The most used pellet in the reactor is A (50%), followed by C (40%) and B (10%).

Table 3.5 summarizes the simulation comparing the results obtained from the model based on transport equations, multiphase and multicomponent systems with the industrial results provided by the studied mill. It appears that the key process parameters, such as metallization,

carburation and production in the model were comparable to the industrial values collected. There are no values in the remaining parameters similar to the industrial averages but were within the confidence interval of the industrial values measured over 30 days.

Table 3.5 - DRI and process parameters evaluated.

Parameters	Average metallization (%)	Average Carburization (%)	Top gas - (CO_2 / $CO+CO_2$) (%)	Top gas - (H_2O / H_2+H_2O) (%)	Pressure Drop (atm)	Production (t/h)
Industrial Data	93.8	2.3	46.1	44.4	0.97	128
Model Result	93.75	2.35	48.11	46.76	1.09	128

Figure 3.2 shows the temperature profile of solids and gas. The results obtained in the simulation are aligned with what is expected for a typical industrial operation. First, the temperatures of solids and gases are close to each other and the highest temperature observed inside the reactor in both cases is slightly lower than the bustle gas temperature because after entering the shaft, the bustle gas expands its volume and subsequently experiences a slight pressure drop. In addition, the regions of higher temperatures in the reduction zone are close to the walls, whereas the cooling zone presents lower temperatures due to the carburization reaction with CH_4, which is endothermic.

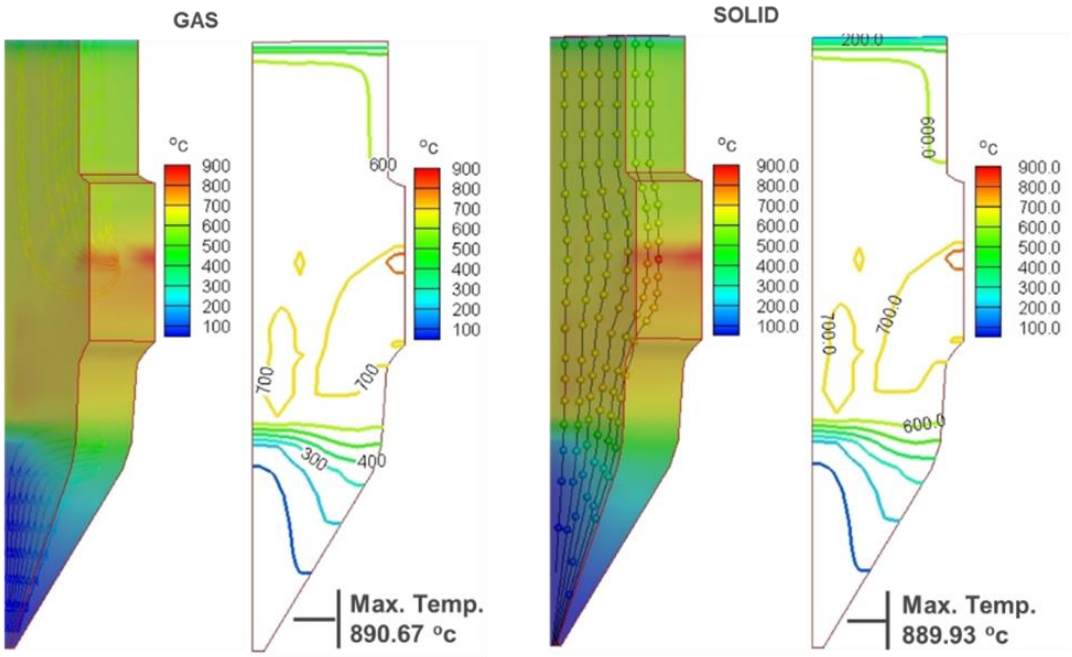

Figure 3.2 - Solid and gas thermal profile.

3.3.2. CI Approach Results

In all tests performed, each of these equations generated a CI that replaced the Eq. 15 and led to different outputs of the solid fraction and consequently permeability. The CIs that result from each equation for different temperature ranges are shown in Table 3.6.

Table 3.6 - Temperature and its relative CI for each equation tested.

Temperature °C	CI1	CI2	CI3	CI4
850	14.33	22.50	1.50	12.76
900	33.33	44.25	23.75	23.48
950	52.33	66.00	46.00	43.20
1000	71.33	87.75	68.25	79.52
1050	90.33	109.50	90.50	146.34

All cases/equations had a version called “Adjusted” that represents the return to the base case's original condition for Dp (pressure drop). This understanding reflects the operational practices that always aim to work within an ideal range of Dp in order to keep operational safety and stability. Thus, all four evaluation cases use equations that correct the solid fraction volume, which decreases the permeability and increases the Dp of the reactor. Therefore, in the adjusted cases, the Dp is reestablished, correcting gas flow and/or temperature, and thus these adjusted cases lead to lower productivity, as shown in Table 3.7.

Table 3.7 - DRI and process parameters for each case evaluated.

	Base case	CI1	Adjusted	CI2	Adjusted	CI3	Adjusted	CI4	Adjusted
Production (t/h)	128.00	128.00	96.50	128.00	104.00	128.00	96.00	128.00	100.50
Dp (atm)	1.030	1.36	1.029	1.26	1.032	1.51	0.979	1.28	1.024
Metalization (%)	93.28	93.89	93.80	93.84	93.70	93.93	93.39	93.73	93.46
$CO_2/(CO+CO_2)$ (%)	46.00	46.88	49.27	46.79	48.53	46.94	49.34	46.71	48.87
$H_2O/(H_2+H_2O)$ (%)	43.96	43.90	43.39	43.93	43.53	43.86	43.54	43.87	43.48

Such numerical simulation results in Table 3.7 were contrasted with the practical experience based on two real situations involving two DR shaft furnace reactors from different locations. In one case, a pellet consumes a CI of 10%, which was replaced by another pellet of the same supplier, but with a CI of 39%. In the other case, the same pellet with a 10% Clustering Index was changed by one with a 13% CI. The impacts in both scenarios were similar. It was necessary to reduce the temperature and flow rate of the bustle gas over a period and, as a result, the furnace productivity decreased. Even though they are different furnaces, dealing with the data in both cases led to a correlation, where each additional 1% CI in the burden would result in a

relative decrease of production around 0.83%. Table 3.8 presents the data from each numerical simulation based on the four equations formulated. Figure 3.3 shows the decrease of production-related to each 1% of CI, aiming to highlight the best value compared to the empirical rule.

Table 3.8 - DRI production loss according to each CI equation.

Equation	Decrease of production t/h	Relative decrease %
CI1	31.5	24.61
CI2	32.0	25.00
CI3	24.0	18.75
CI4	27.5	21.48

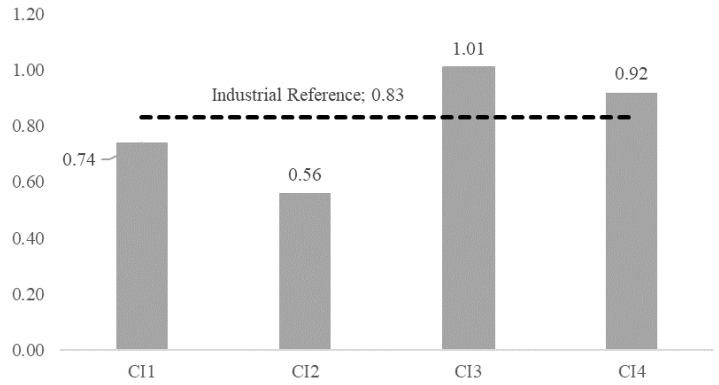

Figure 3.3 - Decrease of production for each 1% Clustering Index.

It can be seen from Table 3.8 and Figure 3.3 that the Equations CI1 and CI4 are the ones that come closest to the industrial value of 0.83%. However, when observing Table 3.6, it is noted that extrapolating the Equation CI4 to temperature values just above 1000 °C would result in CI values above 100%, which is something impossible. Therefore, the most suitable equation considered to represent the impact of the clustering inside the reactor was the Equation CI1.

3.3.3. Temperature Influence on CI

Figure 4.4 depicts the influence of the bustle gas temperature on CI. Each slice of the furnace represented by the letters in Figure 3.4 refers to a simulation made at a specific bustle gas temperature in its steady state. As can be seen, the fraction of solids (clusters) increases with increasing bustle gas temperature, where Equation Cl1 was applied to conduct this investigation. This aspect is in line with the industrial reports of buildup problems (Costa et al., 2013, Voelker, 2019) because clusters usually concentrate. In more severe cases, these clusters

can accumulate inside the furnace and drastically obstruct the permeability, requiring a maintenance cold stop. This is why reactors cannot be found operating at bustle gas temperatures much higher than 1000°C.

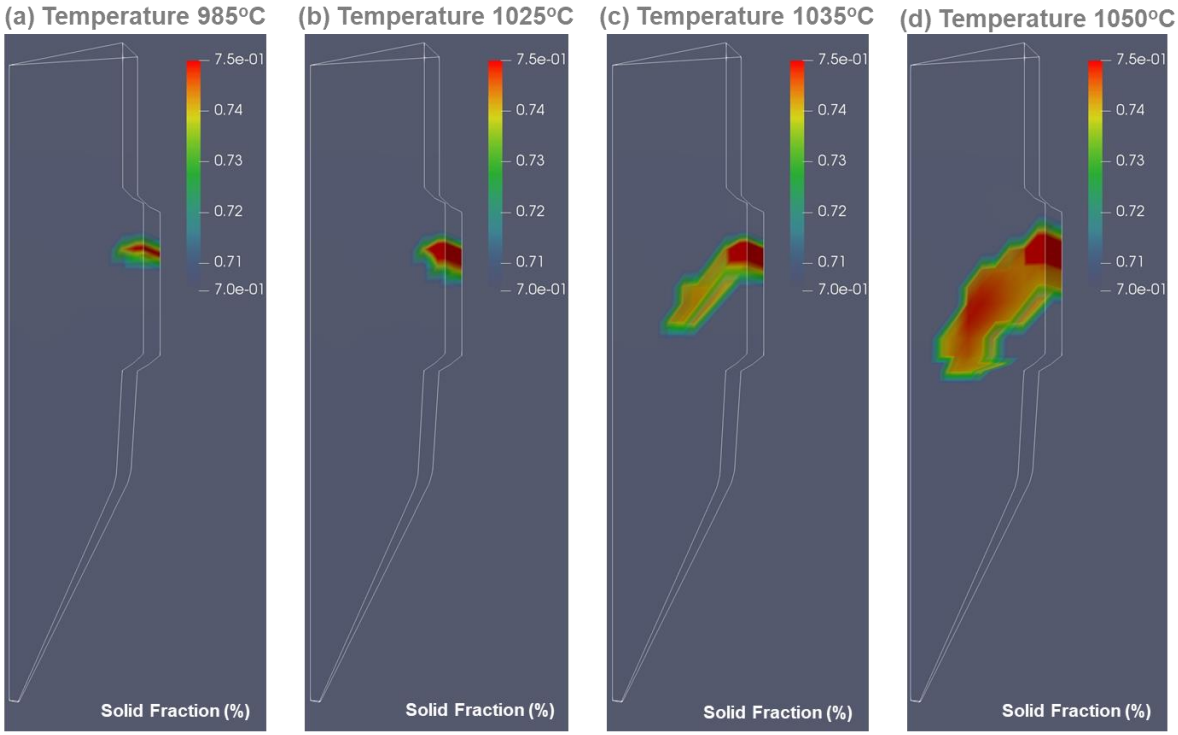

Figure 3.4 - Evolution of solid fraction according to bustle gas temperature simulated: (a) 985°C, (b) 1025°C, (c) 1035°C and (d) 1050°C.

3.4.Conclusions

The experience of seeking literary references about the temperature impact on the formation of the clusters and associating these equations with the solid's fraction volume and their respective bed permeability was novel and successfully tested using an adjusted mathematic approach. Based on this study, new evaluations of potential coating agents may be performed more assertively through laboratory tests and the developed numerical model, saving costs and time with more complex and industrial tests. In addition, from the data obtained with this study, it can be stated that:

- The adaptation of a pre-existing model based on the finite volumes' method focusing on the RD process was suitable to assess the impact of the cluster formation inside a DR shaft furnace reactor.

- From the equations evaluated in this study, the Equation CI1 (CI1 (%) = 0.38 x T (°C) - 308.67) was the one that showed the best adherence to the empirical result of real case studies.
- These equations for clustering modelling used in different temperatures presented the same industrial trend, starting with the reactor walls and going towards the center.

Conflicts of interest

The authors declare no conflicts of interest.

Acknowledgments

The authors would like to thank CAPES-PROEX, CNPq and FAPEMIG for stimulating and supporting research.

References

[1] AHMAN, M. et al. Hydrogen steelmaking for a low-carbon economy: a joint LU-SEI working paper for the HYBRIT project. Lund: Lunds universitet, 2018. (EESS report n. 109).

[2] AJBAR, A.; ALHUMAIZI, K.; SOLIMAN, M. Modelling and parametric studies of direct reduction reactor. Ironmaking & Steelmaking, v. 38, n. 6, p. 401-411, 2011.

[3] AKIYAMA, T.; HOHTA, H.; TAKAHASHI, R.; WASEDA, Y.; YAGI, J. Measurement and modeling of thermal conductivity for dense iron oxide and porous iron ore agglomerates in stepwise reduction. ISIJ International, v. 32, n. 7, p. 829-837, 1992.

[4] ALENCAR, J. Avaliação do efeito da temperatura na morfologia do ferro metálico e na formação da colagem em diferentes tipos de pelotas de redução direta. 2015. Dissertação (Mestrado em Engenharia Metalúrgica, Materiais e de Minas) – Escola de Engenharia, Universidade Federal de Minas Gerais, Belo Horizonte, 2015.

[5] ALENCAR, J.; RESENDE, V.; CASTRO, L. Effect of temperature on morphology of metallic iron and formation of clusters of iron ore pellets. Metallurgical and Materials Transactions B, v. 47, n. 1, p. 85-88, 2016.

[6] ARENS M.; WORRELL E.; EICHHAMMER W.; HASANBEIGI A.; ZHANG Q. Pathways to a low-carbon iron and steel industry in the medium-term- the case of Germany. Journal of Cleaner Production, v. 163, p. 84-98, 2017.

[7] ATSUSHI, M.; UEMURA, H.; SAKAGUCHI, T. Midrex processes. Kobelco Technology Review, v. 29, p. 50-57, 2010.

[8] BATTLE, T. et al. The direct reduction of iron. In: SEETHARAMAN, S. (ed.). Treatise on process metallurgy. [S. l.]: Elsevier, 2014. v. 3, p. 89-176.

[9] BIRD, R.; STEWARTAND, W.; LIGHTFOOT, E. Transport phenomena. NewYork: John Wiley&Sons, 1960. (A Wiley International Edition).

[10] CAPRIOTTI, L. Process parameters. In: CAPRIOTTI, L. Direct reduction process. [S. l.]: Development Maximize Technology, 2012.

[11] COSTA, A.; WAGNER, D.; PATISSON, F. Modelling a new, low CO2 emissions, hydrogen steelmaking process. Journal of Cleaner Production, v. 46, p. 27-35, 2013.

[12] CASTRO, J. et al. Mathematical modeling of the shaft furnace process for producing DRI based on the multiphase theory. REM - International Engineering Journal, v. 71, n. 1, p. 81-87, 2018.

[13] CASTRO, J. et al. Mathematical modeling of the shaft furnace process for producing DRI using self-reducing pellets. In: 2019-SUSTAINABLE INDUSTRIAL PROCESSING SUMMIT, 2019, Flogen Star Outreach. Proceedings […]. [S. l.]: SIPS, 2019. p. 171-172.

[14] DORNDORF, M.; DUARTE, P.; ARGENTA, P.; MAGGIOLINO, S.; MARCOZZI, M. Transforming the steelmaking process. Steel Times International, v.42, n.7, p. 29-32, 2018.

[15] GRISCOM, G.; METIUS, J.; KOPFLE. Coating Agents. Direct from Midrex, Charlotte, n. 2, p. 3-6, Apr./Jun. 2000.

[16] HILLE, V.; REDENIUS, A. SALCOS - schrittweise, flexible Dekarbonisierung auf basis bewährter Technologie. Stahl und Eisen, v.138, n.11, p. 95-101, 2018.

[17] HYBRIT. Fossil-free steel: Summary of Findings from HYBRIT Pre-Feasibility Study 2016–2017. [S. l.]: HYBRIT, 2018. Available at: https://ssabwebsitecdn.azureedge.net/-/media/hybrit/files/hybrit_brochure.pdf. Accessed: 20 may 2020.

[18] INTERNATIONAL ORGANIZATION FOR STANDARDIZATION. ISO 11256: Iron ore pellets for shaft direct-reduction feedstocks - Determination of the clustering index. Genebra: ISO, 2007. 13 p.

[19] KAZEMI, M.; POUR, M.; SICHEN, D. Experimental and modeling study on reduction of hematite pellets by hydrogen gas. Metallurgical and Materials Transactions B, v. 48, n. 2, p. 1114-1122, 2017.

[20] MELAAEN, M. Calculation of fluid flows with staggered and nonstaggered curvilinear nonorthogonal grids-the theory. Numerical Heat Transfer, Part B Fundamentals, v. 21, n. 1, p. 1-19, 1992.

[21] MIDREX. World direct reduction statistics. [S. l.]: MIDREX, 2020. Available at: https://www.midrex.com/insight/ world-dri-production-exceeds-108m-tons-in-2019/. Accessed: 20 May 2021.

[22] NEGRI, E.; ALFANO, D.; ORLANDO, M.; CHIOVETTA, M. Direct reduction of hematite in a moving-bed reactor. Analysis of the water gas shift reaction effects on the reactor behavior. Industrial & Engineering Chemistry Research, v. 30, n. 3, p. 474-482, 1991.

[23] NEUFELD, P.; JANZEN, A.; AZIZ, R. Empirical equations to calculate the transport collision integrals for Lennard-Jones potentials. Journal Chemical Physics, vol. 57, n. 3, p.1100-1102, 1972.

[24] NOURI, S.; EBRAHIM, H.; JAMSHIDI, E. Simulation of direct reduction reactor by the grain model. Chemical Engineering Journal, v. 166, n. 2, p. 704-709, 2011.

[25] PARISI, D.; LABORDE, M. Modeling of counter current moving bed gas-solid reactor used in direct reduction of iron ore. Chemical Engineering Journal, v. 104, n. 1-3, p. 35-43, 2004.

[26] PATANKAR, S. Numerical heat transfer and fluid flow. [S. l.]: CRC Press, 2018.

[27] PEREIRA, J. Avaliação da utilização de diferentes materiais para diminuição da tendência de colagem de pelotas durante o processo de redução direta. 2012. Dissertação (Mestrado em Engenharia Metalúrgica, Materiais e de Minas) – Escola de Engenharia, Universidade Federal de Minas Gerais, Belo Horizonte, 2012.

[28] PINEAU, A.; KANARI, N.; GABALLAH, I. Kinetics of reduction of iron oxides by H2: Part I: Low temperature reduction of hematite. Thermochimica Acta, v. 447, n. 1, p. 89-100, 2006.

[29] PIOTROWSKI, K. et al. Effect of gas composition on the kinetics of iron oxide reduction in a hydrogen production process. International Journal of Hydrogen Energy, v. 30, n. 15, p. 1543-1554, 2005.

[30] REID, R.; PRAUSNITZ, J.; POLING, B. The properties of gases and liquids. New York: McGraw-Hill, 1987.

[31] SHAMS, A.; MOAZENI, F. Modeling and simulation of the MIDREX shaft furnace: reduction, transition and cooling Zones. JOM, v. 67, n. 11, p. 2681-2689, 2015.

[32] TAKENAKA, Y. et al. Mathematical model of direct reduction shaft furnace and its application to actual operations of a model plant. Computers & Chemical Engineering, v. 10, n. 1, p. 67-75, 1986.

[33] THURNHOFER, A. et al. Iron ore reduction in a continuously operated multistage lab-scale fluidized bed reactor-Mathematical modeling and experimental results. Metallurgical and Materials Transactions B, v. 37, n. 4, p. 665-673, 2006.

[34] VALIPOUR, M.; HASHEMI, M.; SABOOHI, Y. Mathematical modeling of the reaction in an iron ore pellet using a mixture of hydrogen, water vapor, carbon monoxide and carbon dioxide: an isothermal study. Advanced Powder Technology, v. 17, n. 3, p. 277-295, 2006.

[35] VENKATESWARAN, V.; BRIMACOMBE, J. Mathematical model of the SL/RN direct reduction process. Metallurgical and Materials Transactions B, v. 8, n. 2, p. 387-398, 1977.

[36] VOELKER, B. Methods for mitigating the buildup of direct reduced iron clusters on the walls of a direct reduction furnace. Depositor: Midrex Technologies. U.S. 2017/0292168A1, Deposit: 12 Apr. 2017. Concession: 6 Aug. 2019.

[37] WILKE, C. A viscosity equation for gas mixtures. The Journal of Chemical Physics, v. 18, n. 4, p. 517-519, 1950.

[38] YI, L.; HUANG, Z.; JIANG, T. Sticking of iron ore pellets during reduction with hydrogen and carbon monoxide mixtures: behavior and mechanism. Powder Technology, v. 235, p. 1001-1007, 2013.

[39] YOU, Y. et al. Investigating the effect of particle shape on the charging process in melter gasifiers in COREX. Powder Technology, v. 351, p. 305-313, 2019.

[40] YU, K.; GILLIS, P. Mathematical simulation of direct reduction. Metallurgical and Materials Transactions B, v. 12, n. 1, p. 111-120, 1981.

[41] ZHANG, B. et al. A comparative study of influence of fluidized conditions on sticking time during reduction of Fe2O3 particles with CO. Powder Technology, v. 225, p. 1-6, 2012.

Capítulo 4. Artigo C - Effect of Coatings and Coating Methods on Cluster Index in Iron Oxide Pellets for Direct Reduction Shaft Furnaces

Jean Philippe Santos Gherardi de Alencar [a,*], *Valdirene Gonzaga de Resende* [a] *and Wander Luiz Vasconcelos*[b]

[a] Ferrous Technology Center, Vale S.A., Nova Lima, MG, Brazil

[b] Metallurgical Department, Federal University of Minas Gerais (UFMG), Belo Horizonte, MG, Brazil

* Corresponding author

Email: jeanpga@gmail.com

Artigo publicado pela revista *Metallurgical and Materials Transactions B* (MMTB)

Received: 08 May 2021 - Accepted: 21 October 2021

Metallurgical and Materials Transactions B, p. 1-11, 2021.

https://doi.org/10.1007/s11663-021-02361-w

ABSTRACT

Coatings have been used for a significant number of years in the Direct Reduction industry and the ISO Cluster Index plays an important role in this context since it allows a better predictability of pellet performance in the industrial process. The present work developed a series of tests and characterization in order to better understand which materials, methods and characteristics would be most relevant to decrease the clustering index. It was noticed that coating on green pellets is worse as compared to the conventional application method which coat the pellets after the hardening process in the pelletizing furnace. In an evaluation of predictive parameters, it was observed that the adhesion index and the sum of SiO_2, Al_2O_3, CaO and MgO content influence the clustering index response variable. Consequently, it was observed that the adhesion index is proportional to the microporosity and mesoporosity of the coating materials. Bauxite was the material that showed the best performance. Its differentials

were the high content of Al_2O_3 combined with its high microporosity/mesoporosity, i.e. pores with diameter up to 50 nm.

Keywords: iron ore pellets; direct reduction; clustering; coating materials.

4.1. Introduction

The world production of sponge iron has been growing and it is already over 100 Mt. In 2019 the highlight of growth was the increase in capacity of coal-based projects in India, added to the Iran and Algeria projects of reactors based on natural gas. New projects to be concluded in 2021 are expected to further increase the production capacity of sponge iron by 7.55 Mt in the world[1]. The aspects that have led these regions of the Middle East, North Africa and Asia to be the most prominent promoters of this route come from the availability of inexpensive natural gas as well as the economic factors of demand for steel[2-4]. However, other factors and regions have also presented longer-term projects that encourage the intense use of the Direct Reduction (DR) and Electric Arc Furnace (EAF) route. In Europe, where there is a regulated carbon market with aggressive CO_2 reduction targets, there are already several projects underway that involve disruptive technologies and greater use of DR, including hydrogen usage[5-10].

Iron ore pellets are the main burden component of the predominant DR reactors, gas-based shaft furnaces. What is expected from the pellets in the shaft furnace is that they have good chemical quality (low gangue content), high physical quality, high metallization degree and low clustering index. The sticking phenomenon (clustering) is critical for reactor permeability and performance. Basically, this phenomenon is defined as the sintering of metallic iron on the surface of the reduced particles[11-17]. Different morphologies can take place depending on the atmosphere and temperature applied and this leads to the operational problems that can vary from gas flow disturbances to reactor shutdown for mechanical maintenance. The higher the reduction temperature, the greater the reduction rate and the greater the proportion of fibrous iron and fresh precipitated iron[12,14,16,18,19]. Some studies have shown that the increase of H_2 proportion in gas composition leads to lower lab Clustering Index (CI) due to the fact that the pore structure of iron obtained by CO reduction is coarser than that by H_2[12,20-22]. However, WANG et al[16] demonstrated another research where increasing hydrogen led to a higher sticking and they attributed this to the fact that the reduction diffusion rate of H_2 was faster, resulting in more contacts of metallic iron phases on the surface of pellets.

Among the existing alternatives to mitigate pellet sticking inside the reactors, there are two practical options: to reduce the bustle gas temperature or using coating agents. The first one is used at critical moments, especially when the clusters inside the reactor are already larger and fixed on the walls. But it is not recommended because working at lower temperatures reduces the kinetics of reduction and consequently decrease the throughput. Then, the use of coatings becomes the main path to prevent the cluster formation without compromising the productivity and DRI (Direct Reduced Iron) quality. The most commonly used materials for coating are Bauxite, Cement, Lime, Limestone, Olivine, Serpentinite, Magnesite, Quartzite, Talc and Bentonite. All of them are refractory oxide minerals rich in elements such as SiO_2, Al_2O_3 and MgO. YI et al[12] compared two types of coating, one rich in SiO_2 and the other rich in CaO and noted that the latter would be more suitable. BASDAG and AROL[15] investigated the effect of the chemical composition of the pellets (basicity), different coating agents and its surface area. The best CI were achieved with a mixture of Limestone and Bentonite, followed by Serpentinite and Bauxite. It was possible to notice that the surface area of the materials, which varied between 5000 and 10000 cm^2/g, was not influential on the results. COLLINS and NORRMAN[23] summarized some studies on the evaluation of coatings by LKAB and found that materials such as Olivine, Magnesite and Cement and its combinations with pozzolanic materials had higher performance to avoid clusters. PEREIRA[24] also made a wide survey of coating materials in two levels of dosage (2.5 and 3.5 kg/t pellet) and the results showed a better performance for coatings with MgO content like Olivine and Serpentine. Thus, given the wide range of coating materials and the lack of clarity about which material has the best chemical or physical characteristics, industrial purchasing decisions has been taken based on economic parameters. Usually the cheapest available coating is the one used, and its dosage is adjusted aiming to obtain an DR operation without technical problems.

In addition, there are some patents and studies that describes different methods to apply coating on the pellets surface[25-30]. Spraying the coating slurry on the conveyor belt when the fired pellet is transported to the stock yard is the normal procedure adopted in the industry.

The need to achieve better levels of productivity and temperature inside the DR reactor continue to impose optimization challenges to mitigate clustering[31-33]. In this context, the present study focused on evaluating different coatings and coating methods on the lab CI in order to seek a better understanding of which fundamental parameters would be more important in the whole process.

4.2.Experimental

The materials used in this study can be divided into two classes: coating materials and iron ore pellets. The iron ore pellets were produced on a pilot scale from a hematite pellet feed. Table 4.1 shows the chemical characterization of the materials that comprised the study, while Table 4.2 demonstrates a quantification of the materials particle size. Regarding the coating materials, the portfolio is diversified, and some chemical characteristics are notorious, as highlighted in bold in the Table 4.1. For example, Bauxite and Al Oxides Mix are rich in Al_2O_3, while Serpentinite and Magnesite Fines stand out, mainly, for their high MgO content. Verdete is a rock with a predominance of SiO_2. Bentonite has high SiO_2 and Al_2O_3. These results were obtained by wet chemical methods, plasma atomic emission spectrometry (ICP-OES) and thermogravimetry.

The granulometric characterization was performed using the Blaine permeability method with help of PC-Blaine-Star from ZEB. For Serpentinites, however, analyses needed to be performed on a Cilas laser granulometer, Model 1064. It can be seen from Table 4.2 that Bentonite is the material with the highest proportion of fine particles, while Serpentinite and Bauxite are the coarsest ones.

Table 4.1. Chemical characterization of the samples (wt.%).

Materials	Fe	SiO_2	Al_2O_3	CaO	MgO	Mn	P	LOI
Pellet	**67.36**	1.99	0.48	1.06	0.05	0.04	0.017	0.06
Bauxite	11.58	7.41	**53.46**	0.01	0.02	0.06	0.005	18.58
Serpentinite	5.12	**50.54**	2.59	0.11	**30.09**	0.10	0.013	6.98
Magnesite Fines	0.30	9.74	0.83	0.41	**42.87**	0.04	0.005	44.58
Al Oxides Mix	0.72	6.97	**79.34**	0.45	**5.70**	-	-	-
Verdete	4.46	**60.02**	15.12	0.09	2.89	0.07	0.068	2.86
Bentonite	4.93	**53.36**	**20.81**	2.01	2.94	0.14	0.022	9.30

Table 4.2. Granulometric characterization of the samples.

Samples	%<0.045 mm
Magnesite Fines	84.2
Bauxite	76.3
Verdete	80.5
Bentonite	98.9
Al Oxides Mix	81.8
Serpentinite	75.1

After chemical and granulometric characterizations, the coating materials were subjected to other investigations to measure properties such as: (i) thermal reactivity, (ii) dispersion degree, (iii) x-ray diffraction, (iv) AI test and (v) porosity.

The thermal reactivity of the materials was evaluated through a fusibility test, which consists of an adapted test based on the standard DIN51730 applied to analyze coal. The fusibility analyzes were conducted in a Hesse Instruments oven, Model HR18. In this case, a briquette sample with a diameter of 3 mm and a height of 3 mm is prepared with the material below 45 µm. The thermal cycle performed consisted of heating at a rate of 10 ºC/min from room temperature to 1000 ºC and after reaching this temperature, the heating rate is reduced to 5 ºC/min until the end of the test. The test can be finished either by the criterion of reaching the maximum oven temperature (1700 °C) or by identifying the fluidity point (1/3 of initial height). The tests were carried out in duplicate.

The dispersion degree test is a typical test of solid-liquid systems for the evaluation of aggregation and dispersion phenomena. Knowing the impact of the interaction of electrostatic charges of solids with the medium is essential to predict slurry behaviors and performances, including solutions for coating materials. In addition, the density or dilution of the slurry is also relevant. A slurry density of coating in the industrial process is usually 1.13 g/cm³. The methodology of dispersion degree used in this test was based on the work of ARAUJO and GALERY[34], where a special glassware is used, with a tap-shaped outlet and at a height above the bottom of the apparatus. The slurry was prepared with a concentration of solids of 2.5 %. After 6 minutes of stirring, the system was at rest for 5 minutes. After this, the dispersed

material and the decanted material were collected, and both were dried to account for the solid mass. The dispersion degree (DG) is given by:

$$DG = \frac{dispersed\ material\ mass}{initial\ mass\ added} * 100\% \qquad \text{(Eq. 1)}$$

The X-ray diffraction analysis was performed in a PANalytical diffractometer (Empyrean model) using a Co tube. The diffractograms were obtained within the range of 5-80° (2θ) with a step size of 0.013°. The crystalline phases were identified using the High Score Plus software.

Based on the characterization, the best coating samples were chosen to follow to next step and subjected to the CI evaluation. Before performing the CI test, the materials were analyzed to determine the AI and the micro and mesoporosity by adsorption of gas. The porosity parameters reported were determined in a NOVA 1000e device from Quantachrome, which uses the principle of adsorption of nitrogen gas on the surface of the solid, using the BET and BJH technique. The overlay map in AI tests is configured in an analysis made through a Zeiss magnifying glass, with variable and controllable lighting system in synergy with a camera connected to the Axiovision SE64 Rel. 4.9.1 SP1 software. Digital image processing provides a covered surface map that estimates the percentage of the covered area.

The coating application was done basically in two ways: (i) conventional method and (ii) alternative method. The first consisted of producing the pellets in the Pot Grate and then applying the coating in the form of a slurry by spraying. Meanwhile, the alternative application method was made at the moment after the consolidation of the green pellets in the pelletizing disc and before loading into the Pot Grate. The coating agent in this case was applied in the form of powder, directly on the pellets, taking into account the same dosage than the conventional one: 3.5 kg of coating per 1 ton of dried pellet. It is important to reinforce that both iron ore pellet source and the coating dosage were kept constant along the work.

Finally, the samples obtained after the final coating application were directed to the CI metallurgical test. The retort and methodology for the reduction followed the same guidelines as the ISO 11256 standard, but there was a change in the maximum reduction temperature, which, in this study, was established at 925 °C.

4.3.Results and Discussion

4.3.1. Characterization of the coating materials

4.3.1.1. Thermal Reactivity

Each coating material was tested in duplicate in the fusibility device. Based on the area, height, width and shape factor of the sample in the cylindrical shape, it is possible to determine different temperatures between the beginning of deformation and the melting of the material. These various temperatures can be summarized in the deformation point and flow point, which are defined as:

- Deformation point: the moment of beginning of softening, characterized by the rounding of the sample edges;
- Flow point: it is the temperature at which the height of the sample reaches 1/3 of the initial height.

The Deformation and Flow points observed are presented in Table 4.3. Deformation point results were written in a range format; since they are determined by the rounding of the corners there are more factors that play a role in the measurements, such as the initial geometric perfection of the specimens. As can be seen in Table 4.3, many materials did not reach the flow point until the temperature of 1600 ° C. Therefore, it was necessary to draw the relative height curves shown in Figure 4.1 to better understand the softening and fluidity aspects of these materials. At each temperature the relative height is measured, which consists of the division between the current height and the initial height of the cylinder. From these analyses, the materials that least flowed and changed with exposure to high temperatures were, in order: Al Oxides Mix, Magnesite Fines, Bauxite, Serpentinite and Verdete.

Table 4.3. Fluidity parameters collected through Fusibility test.

Coating Materials	Deformation Point (°C)	Flow Point (°C)
Magnesite Fines	1337 - 1460	ND
Bauxite	1151 - 1265	ND
Verdete	1123 - 1212	1420
Al Oxides Mix	1562 - 1600	ND

Serpentinite	1236 - 1335	1453

**ND: Not detected up to the maximum temperature of the test (1600°C)*

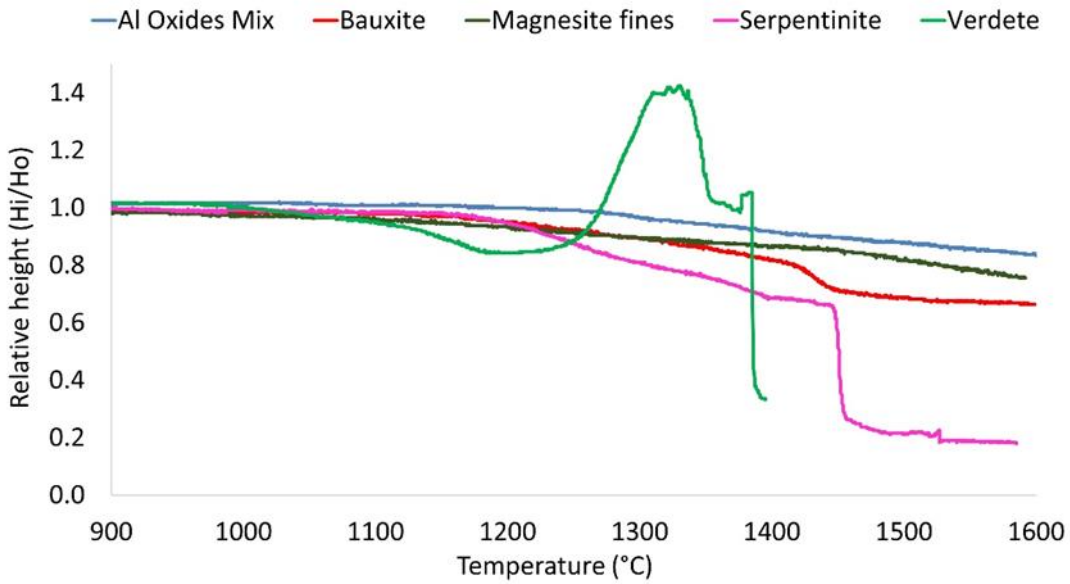

Figure 4.1: Relative height variation of the sample tested as a function of temperature.

4.3.1.2. Dispersion Degree

The DG tests were conducted with combinations of the coating materials and bentonite. Eight refractory materials and two additive conditions (with and without bentonite) were used. Dispersions using bentonite were made using 80 % of the refractory material with 20 % of the binder. The DG is important to evaluate aspects of the DLVO theory. In this theory it is defined that the interaction between particles of colloidal minerals are a function of the Van der Waals forces and the forces between the double electrical layers of the particles. When the particle charges have an identical signal, an electrostatic repulsion occurs which promotes the stabilization of the dispersion[35,36].

The DG tests were performed in duplicate and the average results were expressed in Figure 4.2. It can be seen that materials which showed better dispersion without additives were, in order: Verdete, Serpentinite, Al Oxides Mix, Bauxite and Magnesite Fines.

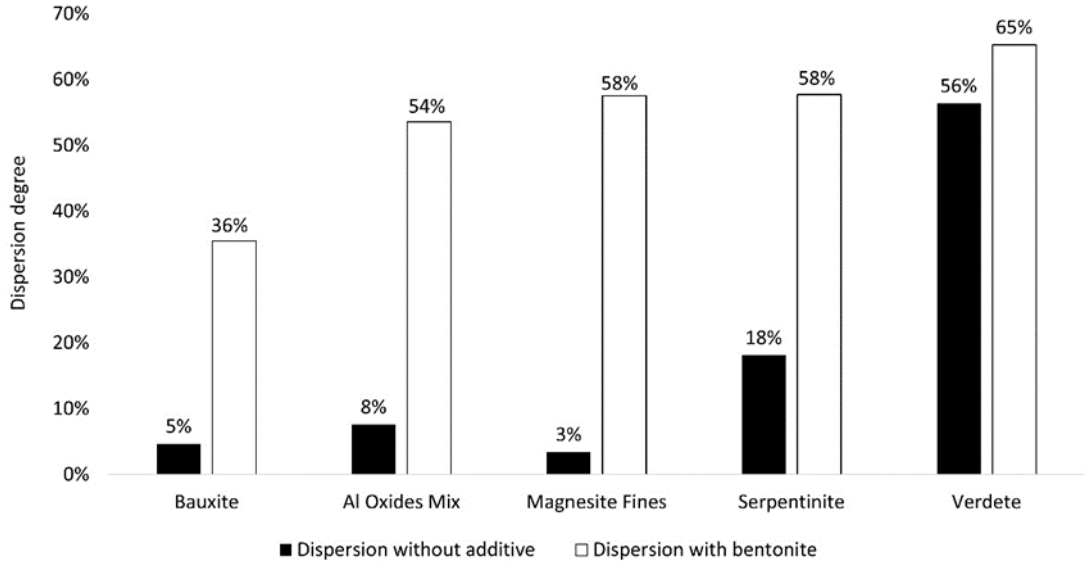

Figure 4.2: DG of the samples with and without bentonite.

Verdete was the most easily dispersed material, which is explained by the high content of quartz, which is an oxide mineral that leads to reactions of superficial hydrolysis in contact with water and thereby increases the level of electrostatic repulsion between its particles.

It is observed that in all experimental points the addition of bentonite provided a significant improvement in dispersion. This fact was also expected since bentonite is an aluminum silicate clay that can absorb its own weight of water several times to form a highly thixotropic colloidal gel. The structure of the gel is derived from the hydrogen bonds that develop between the clay particles[37].

4.3.1.3.X-Ray Diffraction Analysis

X-ray diffraction analyzes were performed on the coating materials. Figure 4.3 shows the major crystalline phases observed in each of the materials which are in line with their chemical composition.

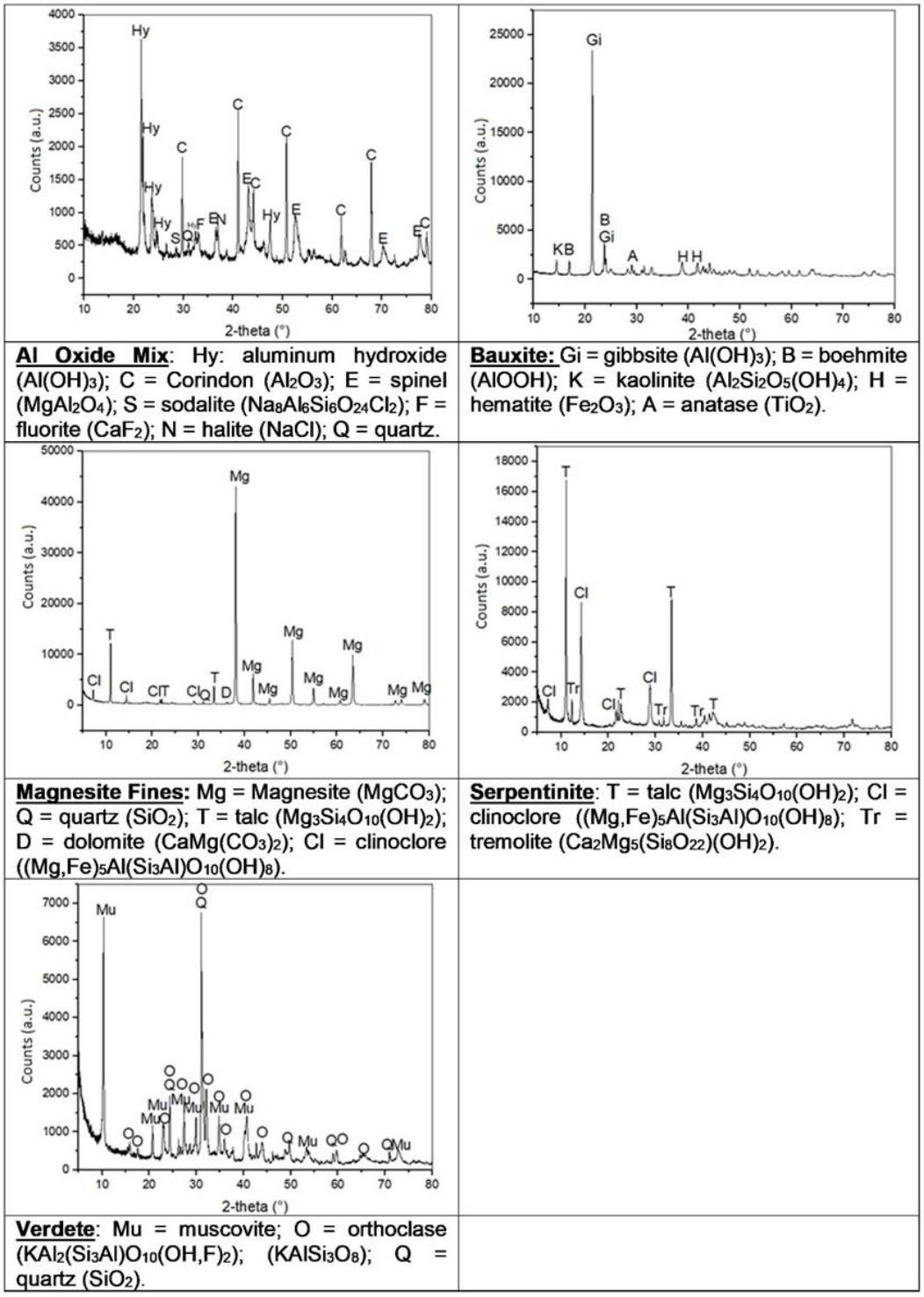

Al Oxide Mix: Hy: aluminum hydroxide ($Al(OH)_3$); C = Corindon (Al_2O_3); E = spinel ($MgAl_2O_4$); S = sodalite ($Na_8Al_6Si_6O_{24}Cl_2$); F = fluorite (CaF_2); N = halite (NaCl); Q = quartz.

Bauxite: Gi = gibbsite ($Al(OH)_3$); B = boehmite (AlOOH); K = kaolinite ($Al_2Si_2O_5(OH)_4$); H = hematite (Fe_2O_3); A = anatase (TiO_2).

Magnesite Fines: Mg = Magnesite ($MgCO_3$); Q = quartz (SiO_2); T = talc ($Mg_3Si_4O_{10}(OH)_2$); D = dolomite ($CaMg(CO_3)_2$); Cl = clinoclore ($(Mg,Fe)_5Al(Si_3Al)O_{10}(OH)_8$).

Serpentinite: T = talc ($Mg_3Si_4O_{10}(OH)_2$); Cl = clinoclore ($(Mg,Fe)_5Al(Si_3Al)O_{10}(OH)_8$); Tr = tremolite ($Ca_2Mg_5(Si_8O_{22})(OH)_2$).

Verdete: Mu = muscovite; O = orthoclase ($KAl_2(Si_3Al)O_{10}(OH,F)_2$); ($KAlSi_3O_8$); Q = quartz ($SiO_2$).

Figure 4.3: X-ray patterns of the coating materials showing the identified phases.

4.3.1.4.Adhesion Index

All coating materials were applied at the surface of the iron ore pellets as a mixture of 80 % of the refractory material and 20 % bentonite. The coating was applied using two different

methods: (i) conventional, applying the coating slurry with a density of 1.13 g/cm³ as a spray on the fired pellets and (ii) alternatively, applying the coating powder directly to the surface of the green pellet before firing in the pelletizing pilot pot grate. In both cases the established dosage was 3.5 kg of coating material for each ton of pellet. Once the pellet manufacturing process and coating application were completed, about 10 representative pellets were collected and subjected to an evaluation of the covering map via optical microscopy. These results were compiled and generated an average value of AI (%). A value of 100 % would mean that the entire surface of the pellet was covered with the coating material. In Figure 4.4, it is possible to find the values obtained for all samples. Note that in all coating applications on green pellets, the value of AI was almost zero. Such perception was possible even at the macroscopic level, because the color of the pellets from this application method was practically the same as the color of pellets that had not received any coating. It is likely that during the firing process the coating was adsorbed to the inner layers when the pellet was shrinking. This phenomenon occurs due to the sintering and densification of the pellet matrix[38]. On the other hand, among conventional applications, it was found that the Bauxite coating was significantly superior to that of the other materials (Figures 4.4 and 4.5).

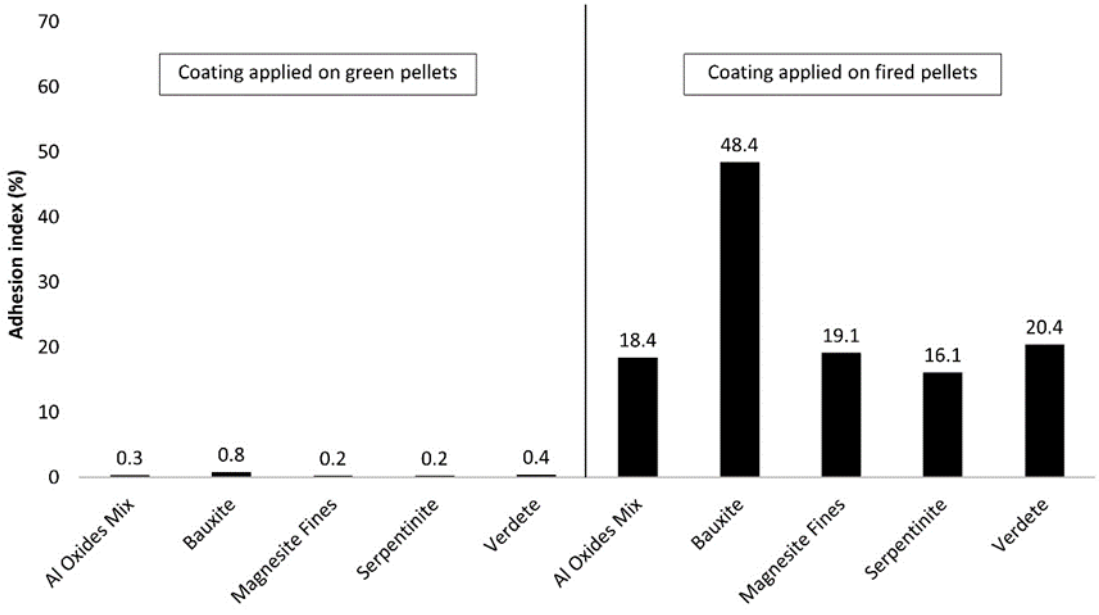

Figure 4.4: Adhesion index of coating materials on pellets.

Serpentinite (a)	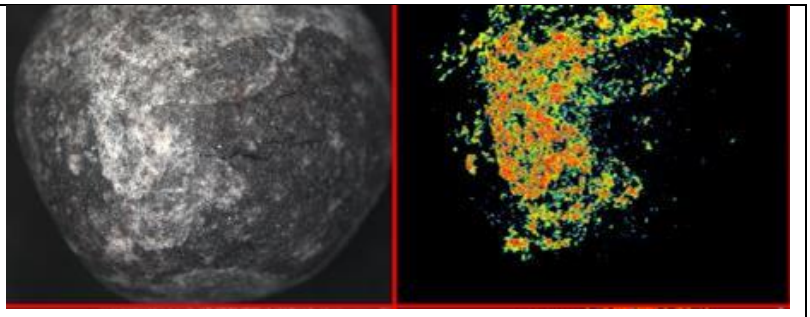
Magnesite Fines (b)	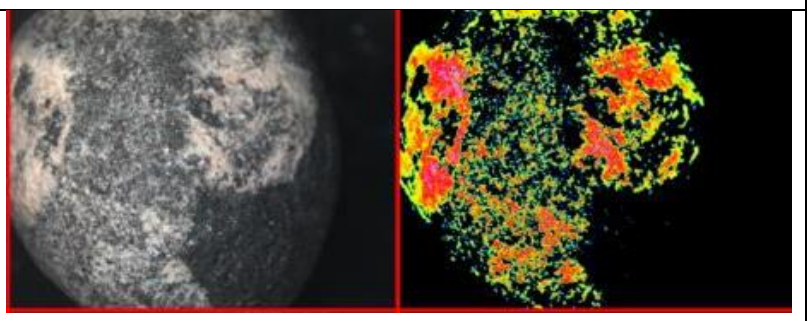
Bauxite (c)	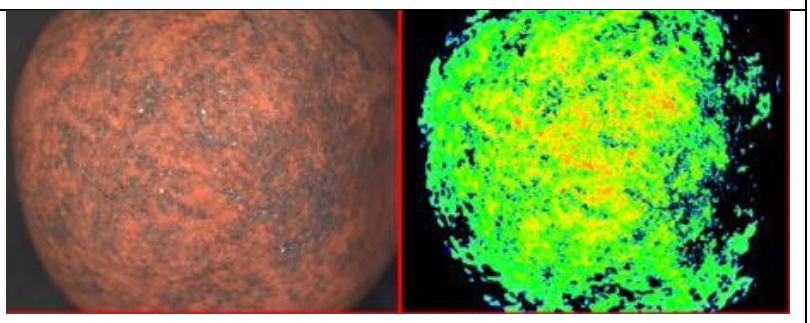
Verdete (d)	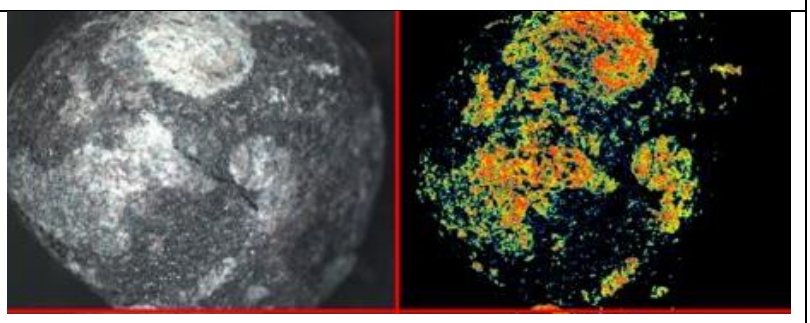
Al Oxides Mix (e)	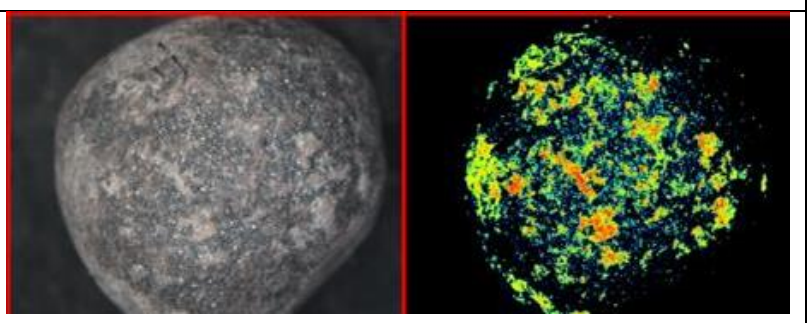

Figure 4.5: Microscopy images of the fired pellets after applying the coating materials: (a) Serpentinite, (b) Magnesite Fines, (c) Bauxite, (d) Verdete and (e) Al Oxides Mix.

4.3.1.5.Porosity

As shown by the granulometric analyses, all coating materials have over 75 % of their particles smaller than 45 μm (Table 4.2). It is believed that the properties of surfaces are very important for coating materials, and the measurement of the specific surface area is fundamental knowledge in the evaluation of new materials; the BET method has been widely used for this purpose. Generally, the presence of pores in a solid material increases its surface area. As for the particle size, the larger the number of small pores, the larger will be the surface area. It was observed on the analyses of the specific surface area of the coating materials (Table 4.4) that Bauxite has the largest while Magnesite Fines have the smallest.

Table 4.4. Specific surface area measured by nitrogen adsorption (BET method).

Coating materials	m^2/g
Magnesite Fines	3.4
Bauxite	116.9
Verdete	16.5
Al Oxides Mix	30.0
Serpentinite	14.7

It was observed that there is a correlation between the specific surface area determined by nitrogen gas adsorption (BET method) with the AI of the coating materials on the surface of the fired pellets, i.e. the highest AI value was observed for Bauxite which showed the largest surface area. Among all analyzed coating materials, Bauxite does not present the largest number of particles below 45 μm (see Table 4.2), indicating that the large surface area may be attributed to high number of small pores present in the particles. This effect specifically associated with small pores can also clarify why BASDAG and AROL[15] couldn't note any correlation between CI and Blaine test results.

4.3.2. Coating Results and Statistical Analysis

4.3.2.1. Clustering Index

The CI tests were performed following the acceptance criteria of the ISO11256 standard. The average results are shown in Figure 4.6 and it can be seen that the CI (%) results of green

pellet coated were always higher than the results obtained in conventional applications (fired pellets), except for Magnesite Fines. Therefore, the expectation already known from the AI results was confirmed that this alternative application method was not effective to maintain the coating on the pellet surface and thus promote a sticking prevention barrier. Regarding the materials, it is possible to see a sequence of those that showed less susceptibility to cluster in the conventional way: Bauxite, followed by the Al Oxides Mix, Serpentinite, Verdete and Magnesite Fines.

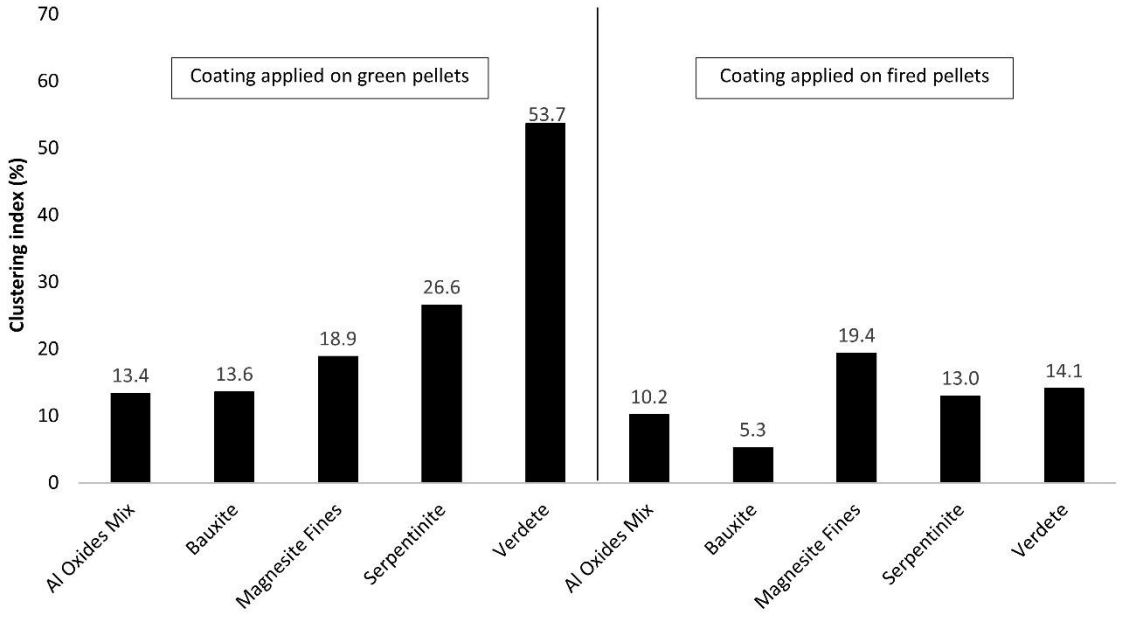

Figure 4.6: CI of the materials evaluated in the alternative and conventional application methods.

4.3.2.2.Statistical Analysis

Multiple regression tests were performed using the Minitab® software to provide the data related to the variables studied. The objective was to assess which of the possible variables would be predictors of the dependent variable CI for cases of conventional coating applications. Within this context, it was tried to use as predictor variables: chemical composition parameters, size distribution, relative height values (from the fusibility test) and the AI. It was found that only the AI value and the sum of the oxides (%SiO_2 + %Al_2O_3 + %CaO + %MgO) were influential in the CI response variable. As can be seen from Table 4.5, as the p-value of both variables was less than 0.05, it can be said that AI and Sum of Oxides are statistical predictors of the CI value. Equation 2 shows the linear regression curve, which reached the adjusted R^2 value of 97.2 %. Therefore, the model found explains 97.2 % of the variability in the CI.

$$CI = 40.9 - 0.246 * Oxides - 0.423 * AI \qquad \text{(Eq. 2)}$$

Table 4.5. Multiple regression test of the CI variable in Minitab®.

Predictor	Coef	SE Coef	T	P
Constant	40.896	2.837	14.42	0.005
Sum of Oxides	-0.24579	0.03079	-7.98	0.015
AI	-0.42304	0.03655	-11.57	0.007

The regression model premises involve the analysis of residuals as to their random distribution, constant variance, independence and normality[39]. Figure 4.7 shows the graphics related to the residuals which prove the requirements previously mentioned. Anderson-Darling method was used as normality test achieving a p-value of 0.057, which confirmed that the residuals are normally distributed.

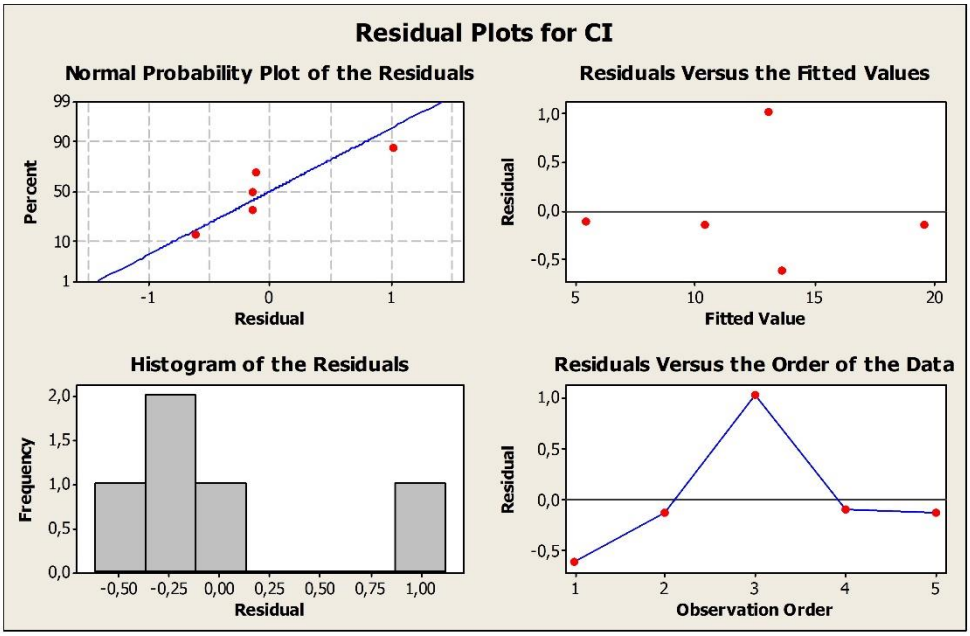

Figure 4.7: Chart of CI analysis regression residuals graphs.

The presence of oxides and its influence on CI is in line with what other works have already shown regarding the efficiency of coatings[12-15,23-25]. The liquidus temperature and refractoriness of these materials depends on the proportion of phases and components. The

higher the ionic bond energy, the higher the liquidus temperature and, consequently, the lesser the chances of the coating losing its physical barrier effect that avoids the contact between the pellets surface[40,41].

Among the predictive values of the CI, we know that the AI is a measurement that is also correlated with other primary characteristics of the samples. Therefore, a new round of multiple regressions considering AI as a response variable was performed, considering as potential predictors the particle size (fraction <0.045 mm), the dispersion degree and the specific surface area. Finally, it was observed that specific surface area (BET method) was the only parameter that has shown to be statistically significant for the AI response. Table 4.6 shows the coefficients found while Equation 3 points to the linear model with adjusted R^2 equal to 92.1 %.

$$AI = 14.2 + 0.283 * SSA \qquad \text{(Eq. 3)}$$

Table 4.6. Multiple regression test of the AI variable in Minitab®.

Predictor	Coef	SE Coef	T	P
Constant	14.208	2.251	6.31	0.008
Specific surface area (SSA)	0.28346	0.0410	6.91	0.006

The residual analysis presented in Figure 4.8 confirms the fulfillment of the statistical requirements. In addition, the p-value obtained in the Anderson-Darling test was 0.069.

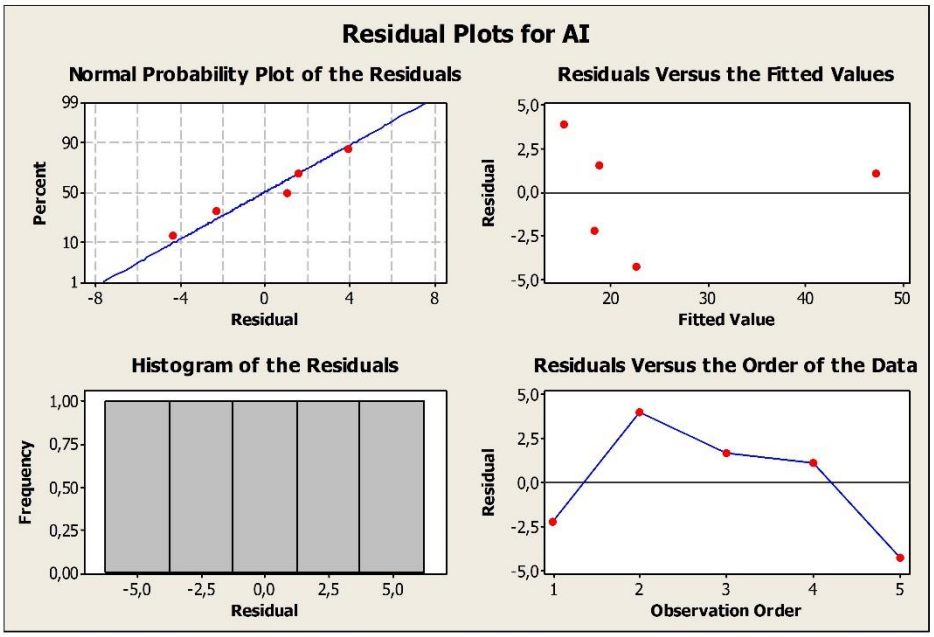

Figure 4.8: Chart of the residual analysis graphs of the AI regression.

The expressive result of correlation between AI and specific surface area is supported by several studies, since this factor has a strong impact on the contact forces between particles and walls[42,43]. The adhesion force tends to decrease with increasing surface roughness to the point where the size of the cavities becomes larger or similar to the size of the particles[44,45]. This is the context of coated pellets, where the pellet substrate cavities are larger or equal in size to some coating particles. In addition, other works from different lines of study show that the greater the presence of micropores, the greater the wettability of the structure and this facilitates the mechanisms of interactions[46,47]. In the case of Bauxite, the higher number of micropores/mesopores results in a greater opportunity for adhesion on the surface of the pellets.

4.4.Conclusions

Experimental investigations on the coating application process were carried out for materials with different characteristics. Based on these results and on the comparison of the available theory on the subject, it is possible to conclude that:

- The attempt to apply coating to the green pellets was unsuccessful, since the pellets after burning practically no longer presented the coating on their surface. This fact was verified with image analysis and corroborated by the metallurgical results of CI.

- The CI values obtained with conventional method application (fired pellets) showed that the material with the best performance was Bauxite, followed by the Al Oxides Mix, Serpentinite, Verdete and Magnesite Fines.
- Among the parameters that were tested as predictors of the CI, only the AI and the total fraction of the oxides SiO_2, Al_2O_3, MgO and CaO were statistically influential in the response variable. The multiple regression equation with these two variables showed an adjusted R^2 of 97.2 %.
- The AI was also assessed as a dependent variable and it was found that the only parameter, among those tested, that proved to impact it was the SSA measured by the nitrogen adsorption (BET method). The regression equation points out that from this SSA parameter it is possible to explain more than 92 % of the AI variability.
- From these conclusions, it is possible to be more assertive in future product development in coating materials and optimize the application methods aiming at greater adherence and refractoriness efficiency that can guarantee low levels of cluster formation under conditions of high temperature and productivity operations in DR reactors.

Conflicts of interest

The authors declare no conflicts of interest.

Acknowledgments

The authors would like to thank CAPES-PROEX, CNPq and FAPEMIG for stimulating and supporting research.

References

[1] MIDREX, World Direct Reduction Statistics. (Midrex Technologies, 2020), https://www.midrex.com/insight/world-dri-production-exceeds-108m-tons-in-2019/. Accessed 12 March 2020.

[2] C. MACHADO: Perspectivas e tendências nos mercados globais de minério de ferro e aço, 2019.

[3] F. MEHMANPAZIR, K. KHALILI-DAMGHANI and A. HAFEZALKOTOB: Resources Policy, 2019, vol. 63, pp. 101409.

[4] H. A. SEVILLA JR: Asian Journal of Middle Eastern and Islamic Studies, 2020, pp. 1-15.

[5] HYBRIT, Hydrogen Breakthrough Ironmaking Technology Brochure. (Hybrit, 2019),https://ssabwebsitecdn.azureedge.net/-/media/hybrit/files/hybrit_brochure.pdf. Accessed 28 April 2020.

[6] H2FUTURE, Green Hydrogen. (Verbund Solutions GmbH, 2018), https://www.h2future-project.eu. Accessed 28 April 2020.

[7] GRINHY, Green Industrial Hydrogen. (Salzgitter Mannesmann Forschung GmbH, 2018), https://www.green-industrial-hydrogen.com. Accessed 28 April 2020.

[8] ARCELORMITTAL, Hydrogen-based steelmaking to begin in Hamburg. (ArcelorMittal, 2020), https://corporate.arcelormittal.com/media/case-studies/hydrogen-based-steelmaking-to-begin-inhamburg. Accessed 28 April 2020.

[9] HYDROGEN COUNCIL, Hydrogen scaling up. (The hydrogen council, 2017), https://hydrogencouncil.com/wpcontent/uploads/2017/11/Hydrogen-scaling-up-Hydrogen-Council.pdf. Accessed 28 April 2020.

[10] EUROPEAN COMMISSION, Energy Efficiency and CO2 Reduction in the Iron and Steel Industry. (EU, 2018), https://setis.ec.europa.eu/system/files/Technology_Information_Sheet_Energy_Efficiency_and_CO2_Reduction_in_the_Iron_and_Steel_Industry.pdf. Accessed 28 April 2020.

[11] M. KOMATINA and H. W. GUDENAU: Metallurgical and Materials Engineering, 2018.

[12] L. YI, Z. HUANG and T. JIANG: Powder Technology, 2013, vol. 235, pp. 1001-1007.

[13] Z. DI, Z. LI, R. WEI, Y. LIU, Q. MENG, T. CHUN, H. LONG, J. LI and P. WANG: Ironmaking & Steelmaking, 2019, vol. 46, n. 2, pp. 159-164.

[14] J. P. S. G. DE ALENCAR, V. RESENDE and L. CASTRO: Metall. Trans. B, 2016, vol. 47, n. 1, p. 85-88.

[15] A. BASDAĞ and A. AROL: Scandinavian journal of metallurgy, 2002, vol. 31, n. 3, pp. 229-233.

[16] G. WANG, J. ZHANG, Y. LI, C. XU and Z. LIU: Powder technology, 2019, vol. 352, pp. 25-31.

[17] R. XU, J. ZHANG, H. ZUO, K. JIAO, Z. HU and X. XING: Journal of Iron and Steel Research International, 2015, vol. 22, n. 1, pp. 1-8.

[18] J. FANG: Theory of Non-Blast Furnace Ironmaking Process, 2002.

[19] J. FANG: Gangtie, 1991.

[20] L. YI, Z. HUANG, T. LI and T. JIANG: Journal of Central South University, 2014, vol. 21, n. 2, pp. 506-510.

[21] J. F. GRANSDEN and J. S. SHEASBY: Canadian Metallurgical Quarterly, 1974, vol. 13, n. 4, pp. 649-657.

[22] S. HAYASHI, S. SAYAMA and Y. IGUCHI: ISIJ International, 1990, vol. 30, n. 9, pp. 722-730.

[23] R. COLLINS and L. NORRMAN: Direct From Midrex, 2001, vol. 2, pp.4.

[24] J. G. PEREIRA. Avaliação da utilização de diferentes materiais para diminuição da tendência de colagem de pelotas durante o processo de redução direta. Master thesis. Federal University of Minas Gerais, 2012.

[25] M. BAHGAT, S. NIAZ, S. LAKDAWALA and H. HANAFY: Journal of Metallurgical Engineering, 2015, vol. 4, pp. 31-41.

[26] J. STERNELAND and P. G. JÖNSSON: ISIJ international, 2003, vol. 43, n. 1, pp. 26-35.

[27] B. VOELKER: U.S. Patent n. 10,370,732, 6 ago. 2019.

[28] J. BERRUN-CASTANON, M. GUERRA-REYES and L. RUIZ-LEAL: U.S. Patent n. 5,181,954, 26 jan. 1993.

[29] M. B. SADDIK and S. N. AHSAN: U.S. Patent Application n. 15/027,857, 1 set. 2016.

[30] M. SADDIK, S. AHSAN, S. LAKDAWALA and H. HANAFY: U.S. Patent Application n. 15/741,935, 12 jul. 2018.

[31] M. ATSUSHI, H. UEMURA and T. SAKAGUCHI: Kobelco Technology Review, 2010, vol. 29, pp. 50-57.

[32] F. MOHSENZADEH, H. PAYAB, Z. ABEDI and M. ABDOLI: Clean Technologies and Environmental Policy, 2019, vol. 21, n. 4, pp. 847-860.

[33] T. BATTLE, U. SRIVASTAVA, J. KOPFLE, R. HUNTER and J. MCCLELLAND: The direct reduction of iron. Elsevier, 2014, pp. 89-176.

[34] A. C. ARAUJO and R. GALÉRY: Encontró Nacional de Tratamento de Minerios e Hidrometalurgia, 1987, vol. 12, pp. 234-48.

[35] T. W. HEALY: Beneficiation of Mineral Fines, 1978, pp. 27-29.

[36] F. A. F. LINS and R. ADAMIAN:. Minerais coloidais, teoria DLVO estendida e forças estruturais, 2000.

[37] B. ABU-JDAYIL: International journal of mineral processing, 2011, vol. 98, n. 3-4, pp. 208-213.

[38] T. KUMAR V. NURNI, H. AHMED, C. ANDERSSON and B. BJÖRKMAN: International Conference on Process Development in Iron and Steelmaking, 2016.

[39] W. HINES, D. C. MONTGOMERY and D. M. BORROR: Probability and statistics in engineering, John Wiley & Sons, 2008.

[40] L. GAN and C. LAI: Metall. Trans. B, 2014, vol. 45, n. 3, pp. 875-888.

[41] C. SCHACHT: Refractories handbook, CRC Press, 2004.

[42] S. RAJUPET, M. SOW and D. J. LACKS: Physical Review E, 2020, vol. 102, n. 1, pp. 12904.

[43] H. MIZES and M. OTT: Particles on Surfaces: Detection: Adhesion and Removal, New York2020, pp. 47.

[44] X. LI M. DONG, D. JIANG, S. LI and Y. SHANG: Powder Technology, 2020, vol. 362, pp. 17-25.

[45] P LIU, C.Q. LAMARCHE, K. M. KELLOGG and S. LEADLEY: AICHE J, 2016, vol. 62, pp. 3529–3537.

[46] Y SUHARTO Y. LEE, J. YU, W. CHOI and K. KIM: Journal of Power Sources, 2018, vol. 376, pp. 184-190.

[47] W. KALLELM. VAN DIJKE, K. SORBIE, R. WOOD, Z. JIANG and S. HARLAND: Advances in Water Resources, 2016, vol. 95, pp. 317-328.

Capítulo 5. Estudo Complementar

Em função dos resultados obtidos nos Capítulos 3 e 4, foi executado uma etapa adicional de testes que tiveram por objetivo buscar uma otimização da aplicação do coating avaliando sua eficiência enquanto mitigador de IC e contrapondo esse ganho com a performance do reator através da simulação numérica. Devido ao fato da aplicação de coating na pelota crua ter sido abaixo das expectativas, optou-se por explorar alternativas de aplicação em dupla camada (tanto na pelota crua quanto na queimada), além de se fazer uso de tratamento térmico. Na Figura 5.1, pode-se ver que o ponto de partida para estes testes, foram pelotas residuais de aplicação de *coating* na pelota crua de Verdete e Mix de Óxidos de Al. Posteriormente, estas pelotas que já estavam queimadas, receberam *coating* de Bauxita através de aplicação de spray de polpa com dosagem de 3,5 kg/t pelota, de maneira igual ao que foi previsto para a aplicação convencional. Por fim, cada par de amostras geradas foi dividido em dois grupos, um no qual a massa de pelotas sofreu tratamento térmico e outro no qual elas seriam armazenadas e destinadas diretamente para o teste de colagem, gerando então um total de quatro novas amostras.

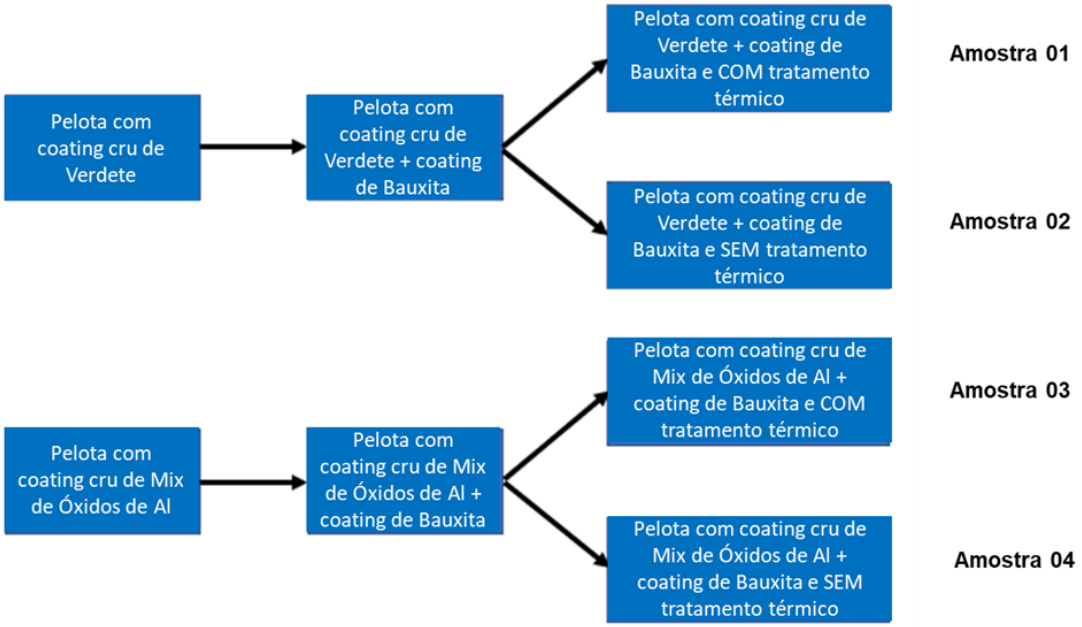

Figura 5.1 - Diagrama de descrição dos testes de otimização.

O tratamento térmico ao qual as pelotas foram submetidas se deu através de um secador infravermelho a temperatura de 400°C. A Figura 5.2 apresenta um quadro com duas fotografias desse secador de esteira que era acoplado a um hopper e tinha potência máxima das placas

emissoras de infravermelho de 60 kW/m². As pelotas, após a aplicação de *coating*, eram submetidas ao secador num ciclo que durava aproximadamente 2 minutos. Cada amostra passou pela correia do secador duas vezes, totalizando 4 minutos de tempo total de secagem do *coating*.

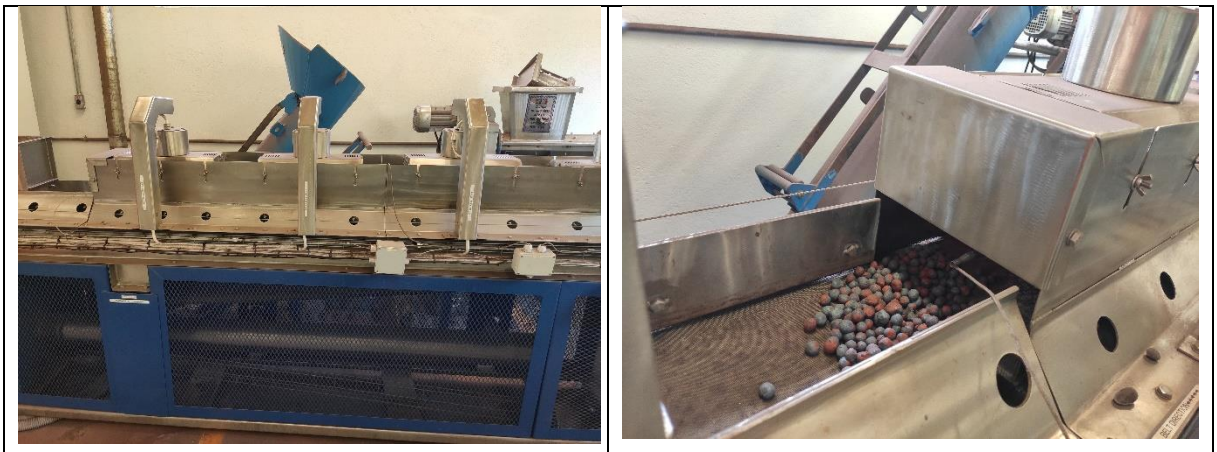

(a) (b)

Figura 5.2 – Quadro de fotografias do secador infravermelho: (a) visão frontal e (b) detalhe do final de curso da esteira.

Na Figura 5.3 observa-se os resultados aferidos na etapa de otimização compilados junto aos resultados anteriores dos materiais individualizados. Os resultados de aplicação complementar de coating seguido de tratamento térmico mostraram ser melhores que cada um dos materiais simples que o compunham. A amostra que tinha aplicação de Verdete apenas na pelota queimada obteve IC de 14,1%, ao passo que quando essa amostra recebeu a camada complementar o valor de IC foi para 24,5% e 7,4% nas condições sem e com tratamento, respectivamente. Por sua vez, a amostra com Mix de Óxidos de Al na pelota queimada atingiu 10,2%, enquanto a amostra que recebeu aplicação externa de Bauxita alcançou 5,2% e 3,2%, esse último com tratamento térmico. É interessante notar que a aplicação da segunda camada de coating sem tratamento térmico foi benéfica apenas a amostra com aplicação prévia de Mix de Óxido de Al, ao que com o tratamento térmico ambas as amostras foram capazes de reduzir o índice de colagem.

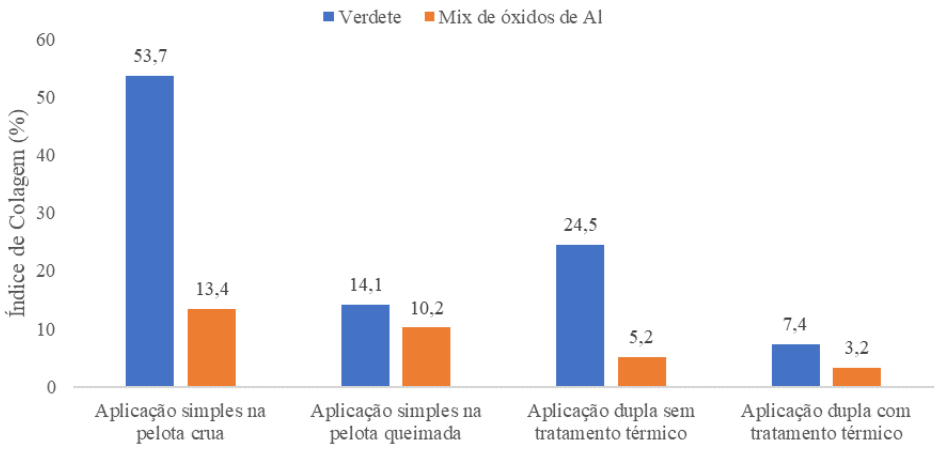

Figura 5.3 - Índice de Colagem após ensaios de otimização.

Nesse contexto, optou-se por comparar no modelo de simulação numérica 3 cenários envolvendo a aplicação de Bauxita: (1) cenário da aplicação simples na pelota crua, (2) cenário de aplicação simples na pelota queimada e (3) cenário de aplicação da Bauxita como complemento da aplicação de Mix de Óxidos com tratamento térmico posterior. Os IC desses cenários eram, respectivamente, 13,6%, 5,3% e 3,2%. A Tabela 5.1 apresenta os resultados dos parâmetros operacionais do reator de forma análoga a Tabela 3.7. Para estabelecer os casos ajustados de cada cenário, o parâmetro de Dp (queda de pressão) foi a referência de balizamento com o Caso Base, também idêntico ao caso base do artigo do Capítulo 3.

Tabela 5.1 – Parâmetros de saída obtidos na simulação numérica dos casos com Bauxita.

	Caso Base	Cenário 1	Ajustado	Cenário 2	Ajustado	Cenário 3	Ajustado
Produção (t/h)	128,0	128,0	108,5	128,0	110,7	128,0	111,0
Dp (atm)	1,030	1,190	1,036	1,170	1,031	1,160	1,030
Metalização (%)	93,28	93,57	93,29	93,48	93,21	93,47	93,26
$CO_2/(CO+CO_2)$ (%)	46,00	46,52	48,08	46,43	47,83	46,40	47,77
$H_2O/(H_2+H_2O)$ (%)	43,96	43,84	43,62	43,83	43,64	43,82	43,64

Pode-se ver que a perda relativa de produção entre o cenário base e cada um dos cenários ajustados fica: 15,23% para o Cenário 1, 13,53% para o Cenário 2 e 13,28% para o Cenário 3. Tais valores remetem a uma reflexão muito importante, pois, uma variação de IC de 5,3% para 3,2% traz um efeito para o processo de RD quase imperceptível de variação de 0,3 t/h de produtividade. Dessa forma, é notório que um esforço de redução do IC como este em questão que teve como origem uma dupla aplicação de *coating* seguida de tratamento térmico não seria compensatória, pois além de prover pouco impacto no processo de redução, acarretaria ainda

em um aumento de custos. Por outro lado, fazer a aplicação de Bauxita na pelota queimada (método convencional) prova-se melhor que a aplicação na pelota crua, pois o custo de insumos seria o mesmo, porém com um desempenho quase 2% melhor de produtividade.

Capítulo 6. Considerações Finais

O presente trabalho se propôs a contextualizar o processo de RD diante do tema da descarbonização da indústria siderúrgica e estudar soluções tecnológicas que pudessem ser aplicadas a fim de diminuir a susceptibilidade das pelotas ao fenômeno de colagem. Através da combinação de levantamentos teóricos, simulações físicas e numéricas, foi possível alcançar resultados que apontam para um melhor entendimento das variáveis que impactam o IC, bem como prever a interferência IC nos aspectos de operação e com isso facilitar sua otimização de processo.

O artigo apesentado no Capítulo 2 abordou o contexto das mudanças climáticas e seu impacto nas criações de mercado regulado de carbono que vem pressionando a indústria siderúrgica, especialmente na Europa. Através dos estudos de caso apresentados nesse artigo verifica-se que já é uma realidade o déficit entre as licenças para emissões de CO_2 e o valor real emitido. Nesse sentido, muitas iniciativas de CDA têm sido levantadas e debatidas com os agentes da siderurgia. Projetos como o SALCOS e HYBRIT são exemplos citados com investimentos já correntes e que visam explorar mais a rota de RD como alavanca para a produção de aço com menor pegada de carbono. O hidrogênio seria o elemento combustível capaz de levar os processos de redução a uma emissão carbono neutra, contudo, seus custos de produção e baixa maturidade de escala tecnológica ainda são obstáculos que precisam ser superados. Apesar das incertezas ainda existentes em relação aos tempos e movimentos das mudanças mais disruptivas na siderurgia, tem-se que a RD é um processo muito viável e conciliável com a meta de zero emissões. Logo, espera-se que este processo cresça e seja comum no futuro e daí a relevância de estudá-lo ainda mais em relação a seus desafios técnicos como o fenômeno da colagem.

O Capítulo 3 mostrou o artigo que se concentrou em apresentar um modelo baseado em equações de transporte aplicados a sistemas reativos multifásicos e multicomponentes que representassem o processo RD levando em consideração o efeito da formação de cachos das pelotas. Além das devidas explicações acerca dos métodos computacionais que resolvem os sistemas acoplados de equações de conservação de momentum, massa e energia, o artigo fez

um levantamento literário de estudos que pudessem fornecer insumos de dados para correlações entre IC e a temperatura. A partir dessa análise, desenvolveu-se nesse trabalho algumas outras equações que correlacionavam o IC com a fração de sólidos dos volumes finitos de controle. Quanto maior a temperatura, maior o IC e maior seria a fração de sólidos de modo a implicar numa menor permeabilidade, fenômeno este esperado na prática operacional. A escolha da melhor equação de IC para aplicação no modelo foi feita com base em dados industriais de perda de produtividade cujo IC da carga era conhecido.

Por outro lado, o Capítulo 4 foi dedicado ao terceiro artigo do trabalho cujo objetivo foi desenvolver uma série de testes e caracterizações visando investigar com uma maior profundidade quais métodos de aplicação, materiais e características são mais relevantes para reduzir o IC laboratorial. Ao se avaliar a reatividade e fluidez dos materiais refratários, percebeu-se que aqueles que se mantiveram mais intactos com o ciclo térmico foram o Mix de Óxidos de Alumínio, Finos de Magnesita e Bauxita. No que diz respeito ao Grau de Dispersão, todos os casos testados com adição de Bentonita tiveram maiores níveis de dispersão quando se comparado com os testes pares sem adição. O método alternativo de coating cuja aplicação se deu na forma de pó aspergido nas pelotas verdes se mostrou de baixa eficácia como mitigador do IC. Por meio das análises de IA foi constatado que pouco se via do material de recobrimento na superfície das pelotas pós-queima quando a aplicação tinha sido feita no método alternativo. Com relação aos resultados de IA do método de aplicação convencional, foi notório que o material que mais aderiu foi às pelotas foi a Bauxita. Numa avaliação estatística de parâmetros preditivos, observou-se que o IA e a soma dos teores de SiO_2, Al_2O_3, CaO e MgO foram influentes na variável resposta IC. Em sequência, ao se procurar outras características que pudessem predizer o IA, constatou-se que a uma relação diretamente proporcional entre os valores de micro e mesoporosidade com o IA. Essa observação é suportada por outros trabalhos que apontam que a maior rugosidade e porosidade favorecem as forças de adesão quando as cavidades são de tamanhos iguais ou maiores que as partículas aderentes, além do fato de que quanto maior a área superficial específica, maior a molhabilidade da estrutura e isso facilita os mecanismos de interação.

Por fim, no Capítulo 5 foi avaliado a aplicação de dupla camada de *coating*, a qual mostrou potencial para menores resultados de IC quando a aplicação final era seguida de tratamento térmico. Todavia, os ganhos obtidos com essas otimizações de aplicação foram relativamente pequenos e ao contrapô-los com os resultados de impacto na produtividade do forno via simulação numérica foi verificado que tais ganhos não se justificariam.

Capítulo 7. Contribuições originais ao conhecimento

As principais contribuições do presente trabalho para o conhecimento científico e tecnológico encontram-se listadas a seguir:

- A criação de um modelo multifásico de multicomponentes que pudesse representar o modelo de RD considerando o fenômeno da colagem foi feita com sucesso e de forma inédita. Não se tinha registros de um modelo semelhante que pudesse representar esse fenômeno de forma quantitativa. As equações utilizadas foram calibradas e selecionadas de acordo com dados industriais que tinham IC da carga e produtividade conhecidas.
- O método de aplicação de coating seco diretamente na superfície de pelotas verdes foi visto como de baixa eficiência. Por meio das análises de imagens pós-queima é possível constatar que há quase nenhum material de coating remanescente na superfície das pelotas e como consequência não há barreira física que evite a formação de cachos. Praticamente todos os IC obtidos com esse método foram piores do que os pares cuja aplicação de coating foi feita pelo método convencional de polpa aspergida na pelota queimada.
- No contexto da série de materiais avaliados, as duas variáveis estatisticamente influentes para o IC foram o IA e a soma dos teores de SiO_2, Al_2O_3, CaO e MgO. Tal constatação é condizente com as premissas teóricas, pois grande parte dos materiais refratários são ricos em óxidos dessa natureza e é de se esperar que quanto mais material refratário presente na superfície da pelota, melhor a barreira física e a capacidade de se evitar os mecanismos de formação de cachos. Contudo, um dos êxitos do trabalho foi varrer várias outras características dos materiais que pudessem justificar os desempenhos desses testes e foi encontrado uma excelente correlação do IA com os resultados da área superficial específica obtidos pela técnica de adsorção de N_2 (método de BET).
- Na etapa complementar de otimização do método de aplicação foi visto que a aplicação de coating em duas camadas: ora na pelota crua e ora na pelota queimada, seguida de tratamento térmico, tende a melhorar o resultado de IC. Entretanto, os ganhos obtidos com essas otimizações de aplicação foram pequenos, sendo que não se justificaria esta aplicação em escala industrial devido ao potencial acréscimo de custos de insumo e processo.

Capítulo 8. Perspectivas de trabalhos futuros

A partir do presente trabalho recomenda-se algumas novas linhas de estudo, como:

- Avaliar diferentes níveis de dosagem de agentes de recobrimento combinado com diferentes níveis de bentonita a fim de otimizar a eficiência técnica e econômica de aplicação.
- Estudar rotas de cominuição de materiais de recobrimento que não utilizem apenas moagem. Por exemplo, simular circuitos que envolvam prensa de rolos para verificar o impacto nas características físicas do material e, consequentemente, na aplicação como coating de pelotas.
- Correlacionar o parâmetro de índice de adesão com a dosagem necessária de coating para recuperação de níveis de índice de colagem satisfatórios para o processo industrial.
- Explorar uma maior gama de materiais refratários através da técnica sol-gel objetivando premissas de qualidade química e física conforme indicado no presente trabalho.
- Avaliar o uso de outros eletrólitos que possam otimizar o grau de dispersão da polpa com material de recobrimento.
- Realizar simulações físicas representativas da redução em ambientes não isotérmicos, mais próximo do *modus operandi* dos reatores industriais.
- Realizar simulações físicas e numéricas representativas do fenômeno de colagem em atmosferas 100% H_2, conforme tendência industrial de descarbonização, a fim de entender as consequências disso na fenomenologia da colagem e prever soluções customizadas.
- Realizar simulações físicas e numéricas do processo de redução em leito fluidizado com foco em prever os aspectos relativos à colagem de partículas.
- Avaliar a influência da basicidade quaternária da pelota, bem como mineralogia do *feed* no índice de colagem.
- Abranger desenvolvimentos de *coating* e métodos de aplicação para outros tipos de aglomerados como, por exemplo, briquetes.